Biogeosciences Discuss., 11, 6461–6517, 2014
www.biogeosciences-discuss.net/11/6461/2014/
doi:10.5194/bgd-11-6461-2014

Biogeosciences Discussions
Open Access

Simulated anthropogenic CO_2 uptake and acidification of the Mediterranean Sea

J. Palmiéri[1,2], J. C. Orr[1], J.-C. Dutay[1], K. Béranger[2], A. Schneider[3], J. Beuvier[4,5], and S. Somot[5]

[1]LSCE/IPSL, Laboratoire des Sciences du Climat et de l'Environnement, CEA-CNRS-UVSQ, Gif-sur-Yvette, France
[2]ENSTA-ParisTech, Palaiseau, France
[3]GEOMAR; Helmholtz-Zentrum für Ozeanforschung Kiel, Germany
[4]Mercator Ocean, Ramonville Saint-Agne, France
[5]CNRM/Météo-France, Toulouse, France

Received: 15 March 2014 – Accepted: 23 March 2014 – Published: 6 May 2014

Correspondence to: J. Palmiéri (julien.palmieri@lsce.ipsl.fr)

Published by Copernicus Publications on behalf of the European Geosciences Union.

Abstract

Constraints on the Mediterranean Sea's uptake of anthropogenic CO_2 are limited, coming only from data-based approaches that disagree by more than a factor of two. Here we simulate this marginal sea's anthropogenic carbon uptake by applying a perturbation approach in a high-resolution regional model. Our model simulates that between 1800 and 2001, basin-wide CO_2 uptake by the Mediterranean Sea has increased by 1.0 Pg C, a lower limit based on the corresponding model evaluation with CFC-12, indicating inadequate simulated deep-water ventilation. Furthermore, by testing a data-based approach (Transit Time Distribution) in our model, comparing simulated anthropogenic CO_2 to values computed from simulated CFC-12 and physical variables, we conclude that the associated basin-wide uptake of 1.7 Pg, published previously, must be an upper bound. Out of the total simulated uptake of 1.0 Pg C, 75 % comes from air–sea exchange into the Mediterranean Sea and 25 % comes from net transport from the Atlantic across the Strait of Gibraltar. Sensitivity tests indicate that the Mediterranean Sea's higher total alkalinity, relative to the global-ocean mean, enhances the Mediterranean's total inventory of anthropogenic carbon by 10 %. Yet the corresponding average anthropogenic change in surface pH does not differ significantly from the global-ocean average, despite higher total alkalinity. In Mediterranean deep waters, the pH change is estimated to be between −0.005 and −0.06 pH units.

1 Introduction

The Mediterranean region will be particularly affected by climate change (Giorgi, 2006; The MerMEX group, 2011; Diffenbaugh and Giorgi, 2012). This region, currently classified as semiarid to arid, is projected to become warmer and drier (Gibelin and Déqué, 2003; Giorgi and Lionello, 2008) amplifying existing water resource problems. At the same time, already heightened anthropogenic pressures are expected to intensify further (Attané and Courbage, 2001, 2004). It has been proposed that the Mediterranean

BGD
11, 6461–6517, 2014

Sea will experience amplified acidification relative to the global average surface ocean (Touratier and Goyet, 2009, 2011). The Mediterranean Sea is able to absorb relatively more anthropogenic CO_2 per unit area for two reasons: (i) its higher total alkalinity gives it greater chemical capacity to take up anthropogenic CO_2 and neutralize acid and (ii) its deep waters are ventilated on relatively short time scales, allowing deeper penetration of this anthropogenic tracer. However the quantity of anthropogenic CO_2 that has been absorbed by the Mediterranean Sea remains uncertain. This quantity cannot be measured directly because the anthropogenic component cannot be distinguished from the much larger natural background. Instead it has been estimated indirectly from observable physical and biogeochemical quantities.

Several indirect methods have been developed, some of which have been compared using the same data sets along basin-wide transects in the Mediterranean Sea. Their first comparison (El Boukary, 2005) revealed large differences between methods. With data from a 1995 transect on the METEOR (M31/1), El Boukary estimated with two methods that the Mediterranean Sea has absorbed 3.1 and 5.6 Pg C, but he concluded that even the lower value was an overestimate. Later, data from a transbasin transect in 2001 (METEOR M51/2) was used by two independent studies to estimate anthropogenic CO_2. In the first, Schneider et al. (2010) used that data with the Transit Time Distribution approach (TTD from Waugh et al., 2006), a back calculation method based on CFC-12 derived mean age of water masses. For the second, Touratier and Goyet (2011) used their TrOCA (Touratier et al., 2007) approach that relies on measured O_2, dissolved inorganic carbon (C_T), and total alkalinity (A_T). Anthropogenic carbon estimated with TrOCA is always greater than that from TTD (Fig. 1), with more than a factor of two difference both in the Western basin below 500 m depth and in the Eastern basin between 500 and 1500 m. These large differences in estimated concentrations further result in opposing estimates for the net transport across the Strait of Gibraltar. With TROCA, the Mediterranean Sea appears to export anthropogenic carbon to the Atlantic Ocean, whereas with TTD, net calculated exchange is in the opposite direction (Schneider et al., 2010; Aït-Ameur and Goyet, 2006; Huertas et al., 2009; Flecha

BGD
11, 6461–6517, 2014

et al., 2011). These large discrepancies between results from currently used data-based methods fuel a debate about the quantity of anthropogenic carbon that is taken up by the Mediterranean Sea.

Here we take another approach by simulating anthropogenic CO_2 uptake of the Mediterranean Sea. Unlike simulations for the global ocean, we cannot rely on coarse-resolution global models because they do not resolve fine-scale bathymetry and circulation features that are critical for the Mediterranean Sea. This semi-enclosed marginal sea is separated into the eastern and the western basins by the Strait of Sicily (Fig. 2). Each of these basins has critical circulation features that are often heavily influenced by bathymetry. For example, Atlantic Water (AW) enters the Mediterranean Sea at the surface via the narrow Strait of Gibraltar and flows counter-clockwise along the coast. Surface-water circulation patterns are influenced by deep- and intermediate-water formation driven by strong winds, which are themselves steered and intensified by surrounding mountainous topography. Deep and intermediate waters are formed in 4 major areas: the Rhodes gyre, where the Levantine Intermediate Water (LIW) originates; the Gulf of Lions and the nearby Ligurian Sea in the Liguro-Provençal sub-basin, which together produce Western Mediterranean Deep Water (WMDW); and two adjacent regions, south of the Adriatic Sea and south of the adjacent Aegean Sea, which together produce Eastern Mediterranean Deep Waters (EMDW). Also influencing the deep circulation is the Mediterranean Outflow Water (MOW), a complex mixture of different intermediate and deep waters outflowing at the Strait of Gibraltar underneath the incoming AW.

To capture these and other key features, we used a high-resolution circulation model of the Mediterranean Sea forced by high resolution air–sea fluxes, interannually varying Atlantic Ocean boundary conditions, and realistic land freshwater inputs. This regional circulation model is combined with a computationally efficient perturbation approach (Sarmiento et al., 1992) to model anthropogenic CO_2 in the Mediterranean Sea. This geochemical approach simulates only the change in CO_2 uptake due to anthropogenic perturbation, assuming that the natural carbon cycle is unaffected by the increase in

BGD
11, 6461–6517, 2014

CO_2. For efficiency, it relies on a formulation that relates surface-water changes in the partial pressure of carbon dioxide (δpCO_2) to those in dissolved inorganic carbon (δC_T). By focusing only on the C_T perturbation, it needs just one tracer and one simulation that covers only the industrial period. Thus it circumvents the need for the prequisite simulation of the natural carbon cycle, which requires many tracers and a much longer simulation to allow modeled tracer fields to reach near steady-state conditions.

Our goal here is to use these simulations to help bracket the Mediterranean Sea's uptake of anthropogenic CO_2 as well as its net transport across the Strait of Gibralter, while exploring how this marginal sea's heightened total alkalinity affects anthropogenic CO_2 uptake and corresponding changes in pH.

2 Methods

Anthropogenic CO_2 simulations were made offline with circulation fields from the NEMO circulation model. The same approach was used to make simulations of CFC-12 in order to evaluate modeled circulation, which heavily influences penetration of both of these passive transient tracers.

2.1 Circulation model

The regional circulation model NEMO-MED12 (Beuvier et al., 2012a) is a Mediterranean configuration of the free-surface ocean general circulation model NEMO (Madec and The-NEMO-Team, 2008). Its domain includes the whole Mediterranean Sea and extends into the Atlantic Ocean to 11°W; it does not include the Black Sea (Fig. 2). The horizontal model resolution is around 7 km, adequate to resolve key mesoscale features. Details of the model and its parametrizations are given by Beuvier et al. (2012a). NEMO-MED12 has been used to study the WMDW formation (Beuvier et al., 2012a), the response of the mixed layer to high-resolution air–sea forcings (Lebeaupin Brossier et al., 2011), and the transport across the Strait of Gibral-

BGD
11, 6461–6517, 2014

tar (Soto-Navarro et al., 2014). NEMO-MED12 is descended from a suite of Mediterranean regional versions of OPA and NEMO used by the French modelling community: OPAMED16 (Béranger et al., 2005), OPAMED8 (Somot et al., 2006), NEMO-MED8 (Beuvier et al., 2010).

The physical simulation used here is very close to that described in Beuvier et al. (2012b). It is initiated in October 1958 with temperature and salinity data representative of the 1955–1965 period using the MEDATLAS dataset (MEDAR/MEDATLAS-Group 2002, Rixen et al., 2005). For the Atlantic buffer, initial conditions are taken from the 2005 World Ocean Atlas for temperature (Locarnini et al., 2006) and salinity (Antonov et al., 2006). Boundary conditions are also needed to specify physical forcing for the atmosphere, freshwater inputs from rivers and the Black Sea, and exchange with the adjacent Atlantic Ocean. For the atmosphere, NEMO-MED12 is forced with daily evaporation, precipitation, radiative and turbulent heat fluxes, and momentum fluxes from the ARPERA dataset (Herrmann and Somot, 2008), all over the period 1958–2008. The ARPERA forcing constitutes a 56 year, high-resolution forcing (50 km, daily data) with a good temporal homogeneity (see Herrmann et al. (2010) for more details about the post-2001 period). The SST-relaxation and water-flux correction terms are applied as in Beuvier et al. (2012a). River runoff is derived by Beuvier et al. (2010, 2012a) from the interannual dataset of Ludwig et al. (2009) and Vörösmarty et al. (1996). Freshwater input from the Black Sea follows runoff estimates from Stanev and Peneva (2002). Exchange with the Atlantic is modelled through a buffer zone (see Fig. 2) between 11°W and the Strait of Gibraltar, where the model's 3-D temperature and salinity fields are relaxed to the observed climatology (Locarnini et al., 2006; Antonov et al., 2006) while superimposing anomalies of interannual variations from the ENSEMBLES reanalysis performed with a global version of NEMO (Daget et al., 2009). To reproduce the monthly cycle of the Mediterranean Sea's water volume, we restore the total sea-surface height (SSH) in the Atlantic buffer zone toward the monthly climatological values of the GLORYS1 reanalysis (Ferry et al., 2010)

BGD
11, 6461–6517, 2014

The atmospheric forcing used by Beuvier et al. (2012b) does not include modifications to improve dense water fluxes through the Cretan Arc, which plays a critical role in deep-water formation during the Eastern Mediterranean Transient (EMT). As detailed by Roether et al. (1996, 2007), the EMT was a temporary change in the Eastern Mediterranean Deep Water (EMDW) formation that occurred when the source of this deep water switched from the Adriatic Sea to the Aegean Sea during 1992–1993. Beuvier et al. (2010) showed that a previous simulation with the circulation model NEMO-MED8 (1/8° horizontal resolution) was able to reproduce a transient in deep-water formation as observed for the EMT, but the simulated transient produced less EMDW. Beuvier et al. (2012b) later made a simulation with NEMO-MED12 with compariable forcing between October 1958 and December 2012. To improve the characteristics of the simulated EMT, namely the density of newly formed EMDW during 1992–1993, its weak formation rate, and its shallow spreading at 1200 m, we made here a sensitivity test with modified forcing. For that, we modified the ARPERA forcings over the Aegean sub-basin, increasing mean values as done by Herrmann et al. (2008) to study the Gulf of Lions. More specifically, during November to March in the winters of 1991–1992 and 1992–1993, we increased daily surface heat loss by 40 $W m^{-2}$, daily water loss by 1.5 $mm day^{-1}$, and the daily wind stress modulus by 0.02 $N m^{-2}$. That resulted in average wintertime increases in heat loss (+18 %), water loss (+41 %), and wind intensity (+17 %) over the Aegean sub-basin. The increased heat and water losses allow NEMO-MED12 to form denser water masses in the Aegean Sea during the most intense winters of the EMT, while increased wind stress drives more intense mixing via winter convection. Furthermore, enhanced convection accelerates the transfer of surface temperature and salinity perturbations into intermediate and deep layers of the Aegean Sea. In summary for this study, the physical model forcing is identical to that from Beuvier et al. (2012b), except for the enhanced forcing during the two winters mentioned above.

BGD
11, 6461–6517, 2014

2.2 Passive tracer simulations

2.2.1 CFC-12

The trace atmospheric gas CFC-12 has no natural component. Being purely anthropogenic, its atmospheric concentration has increased since the 1930's and has leveled off in recent decades. Although sparingly soluble, it enters that ocean by gas exchange. There it remains chemically and biologically inert, tracking ocean circulation and mixing. Precise measurements of CFC-12 along several trans-Mediterranean sections make it particularly suited for evaluating these regional model simulations. To model CFC-12, we followed protocols from Phase 2 of the Ocean Carbon Cycle Model Intercomparison Project (OCMIP-2) as described by Dutay et al. (2002). For the air-to-sea flux of CFC-12 (F_{CFC}), we used the standard formulation for a passive gaseous tracer

$$F_{CFC} = k_w(C_{eq} - C_{surf}) \quad (1)$$

where k_w is the gas transfer velocity (also known as the piston velocity), C_{surf} is the simulated sea-surface concentration of CFC-12, and C_{eq} is the atmospheric equilibrium concentration. That is,

$$C_{eq} = \alpha p\mathrm{CFC} \quad (2)$$

where α is the CFC-12 solubility, a function of local seawater temperature and salinity (Warner and Weiss, 1985), and pCFC is the atmospheric partial pressure of CFC-12 computed from the atmospheric mole fraction in dry air. Here we assume atmospheric pressure remains at 1 atm neglecting spatiotemporal variations. The gas transfer velocity is computed from surface-level wind speeds (u) from the ARPERA forcing following the Wanninkhof (1992, Eq. 3) formulation

$$k_w = au^2 \left(\frac{Sc}{660}\right)^{-1/2} \quad (3)$$

BGD
11, 6461–6517, 2014

where $a = 0.31$ and Sc is also the CFC-12 Schmidt number computed following Wanninkhof (1992, Table A1).

Regarding lateral boundary conditions, for the Atlantic buffer zone (between 11°W and Strait of Gibraltar), we assume that net exchange at the boundary may be neglected while relying on atmospheric exchange of this rapidly equilibrating tracer as the dominant factor.

2.2.2 Anthropogenic CO_2

To model anthropogenic CO_2 in the Mediterranean Sea, we use the perturbation approach (Siegenthaler and Joos, 1992; Sarmiento et al., 1992). This classic approach uses a simple relationship between the change in surface-ocean pCO_2, which is needed to compute the air–sea CO_2 flux, and the change in C_T. Such a relationship is necessary for carbon dioxide, unlike for CFC-12, because as CO_2 dissolves in the ocean it does not simply remain as a dissolved gas; it dissociates into two other inorganic species, bicarbonate and carbonate ions. When modeling only the change in the total of the three species (δC_T), the simple relationship that is used allows models to carry only that perturbation tracer.

In the perturbation approach, the geochemical driver is the atmospheric change in carbon dioxide. As written by Sarmiento et al. (1992), that change in terms of the partial pressure of carbon dioxide in moist air is

$$\delta pCO_{2_a} = \left(pCO_{2_a} - pCO_{2_{a,0}}\right)(1 - e_s/p_a) \quad (4)$$

For the model simulation, the two pCO_2 terms (in µatm) on the right side of the equation are identical to xCO_2 (in ppm), although units differ, because they both refer to dry air and because the perturbation approach assumes a total atmospheric pressure of 1 atm. Of those two terms, $pCO_{2_{a,0}}$ is the preindustrial reference value of 280 µatm (i.e., $xCO_2 = 280$ ppm) and pCO_{2_a} is the prescribed atmospheric xCO_2 obtained from a spline fit to observations from the Siple ice core data and atmospheric CO_2 measurements from Mauna Loa, which together span 1800.0 to 1990.0 (Enting et al., 1994),

BGD
11, 6461–6517, 2014

combined with the 12 month smoothed Manua Loa atmospheric measurements between 1990.5 to 2009.0 (GLOBALVIEW-CO_2, 2010). The final term in Eq. (4) uses the saturation water vapor pressure e_s and the total atmospheric pressure at sea level p_a to convert partial pressure in dry air to that in wet air as needed to compute the air–sea flux.

The modeled air–sea flux of anthropogenic carbon F_{CO_2} follows the standard formulation

$$F_{CO_2} = K_{CO_2}(\delta pCO_{2_a} - \delta pCO_{2_o}) \quad (5)$$

where K_{CO_2} is a gas transfer coefficient, δpCO_{2_a} is described above, and δpCO_{2_o} is the anthropogenic perturbation in surface-water pCO_2 relative to its reference value in 1800. For the gas transfer coefficient, $K_{CO_2} = \alpha k_w$, where α is the CO_2 solubility (Weiss, 1974) and k_w is as in Eq. (3) except that Sc is for CO_2 (Wanninkhof, 1992, Table A1).

The δpCO_{2_o} term is not modeled explicitly but is calculated from the only tracer that is carried in the model, δC_T. The standard formulation from Sarmiento et al. (1992) is based on their finding that the relationship between the ratio $\delta pCO_{2_o}/\delta C_T$ and δpCO_{2_o} is linear, for a given temperature and at constant total alkalinity.

$$\frac{\delta pCO_{2_o}}{\delta C_T} = z_0 + z_1\,\delta pCO_{2_o} \quad (6)$$

where the intercept z_0 and slope z_1 terms are each quadratic functions of temperature. That equation is then rearranged for the model calculation.

$$\delta pCO_{2_o} = \frac{z_0\,\delta C_T}{1 - z_1\,\delta C_T} \quad (7)$$

To allow for a starting value of $pCO_{2_{a,0}}$ that is different than 280 ppm, Lachkar et al. (2007) introduced two corrective terms

$$\delta pCO_{2_o} = \frac{z_0\left[\delta C_T + \delta C_{T,corr}\right]}{1 - z_1\left[\delta C_T + \delta C_{T,corr}\right]} - pCO_{2_{a,corr}} \quad (8)$$

BGD
11, 6461–6517, 2014

where the first correction factor is

$$pCO_{2_{a,corr}} = pCO_{2_{a,0}} - pCO_{2_{a,ref}} \quad (9)$$

determined from the starting xCO_2 in the initial year (1800), i.e., $pCO_{2_{a,0}} = 287.78$ ppm, and same reference $pCO_{2_{a,ref}} = 280$ ppm. With that result, the second correction factor is

$$\delta C_{T,corr} = \frac{pCO_{2_{a,corr}}}{z_0 + z_1\, pCO_{2_{a,corr}}} \quad (10)$$

These two minor corrections do not change the way z_0 and z_1 are computed, but they do slightly alter their use in the model simulations, using Eq. (8) instead of Eq. (7).

Equations for the linear regression coefficients z_0 and z_1 are computed in four steps: (i) estimate the initial preindustrial $C_{T,0}$ as a function of temperature from carbonate system thermodynamics, assuming air–sea equilibrium between the atmosphere ($pCO_{2_{a,0}} = 280$ ppm) and the surface ocean, constant global-average surface total alkalinity (2300 µmol kg^{-1}), constant salinity (35 psu), and varying temperatures across the observed range; (ii) increase incrementally the pCO_{2_a} from 280 to 480 ppm, and recompute the C_T as a function of temperature for each increment; (iii) use those results with Eq. (6) to compute z_0 and z_1 for each temperature; and (iv) fit each of z_0 and z_1 to a quadratic function of temperature. With this approach, Sarmiento et al. (1992) found that Eq. (6) fit exactly calculated values to within 1 % when $\delta pCO_{2_o} \leq 200$ ppm.

The constant value of total alkalinity used in the standard perturbation approach detailed above is the area-weighted mean for the global ocean. That approach with Eq. (8), which we refer to as GLO, will produce biased results for the Mediterranean Sea whose average surface total alkalinity is 10 % greater. Thus we made a second simulation (MED), where z_0 and z_1 that were used with Eq. (8) were computed following the same 4-step procedure as above, except that we replaced the area-weighted surface average total alkalinity for the global ocean (2300 µmol kg^{-1}) with that for the Mediterranean Sea (2530 µmol kg^{-1}).

BGD
11, 6461–6517, 2014

Finally, to test how variable total alkalinity may affect simulated results, we made a third simulation (VAR). The perturbation approach was designed for the global, open-ocean waters where total alkalinity varies relatively little, e.g., from 2243 to 2349 $\mu mol\,kg^{-1}$ in the zonal mean of the GLODAP gridded data product (Key et al., 2004). Spatial variations of surface total alkalinity in the Mediterranean Sea are more than twice as large, e.g., varying from 2375 to 2625 $\mu mol\,kg^{-1}$ between western and eastern margins. To account for variability in Mediterranean total alkalinity, we exploited its tight relationship with salinity derived from the METEOR M51/2 transbasin section by Schneider et al. (2007)

$$A_T = 73.7\,S - 285.7 \tag{11}$$

where S is the model's surface salinity and A_T is its computed surface total alkalinity. This equation thus takes much of the A_T spatial variablity into account (Fig. 3), although it is expected to be inaccurate near river mouths, where fresh waters with high total alkalinity are delivered to the Mediterranean Sea. This equation also implies that computed A_T varies temporally with simulated salinity.

For VAR to take into account variable salinity (total alkalinity) as well as variable temperature, while maintaining adequate precision, we made 2 types of modifications to the standard equations. First, we replaced Eq. (6) with a direct relationship between $\delta pCO_{2,o}$ and δC_T but with a cubic formulation instead of a linear formulation, i.e., implying an additional coefficient.

$$\delta pCO_{2,o} = 0 + z_1\,\delta C_T + z_2\,\delta C_T^2 + z_3\,\delta C_T^3 \tag{12}$$

Then for each of three coefficients, we replaced the former two equations, quadratic in temperature T, with three equations, cubic in T and S.

$$\begin{aligned} z_1 &= a_0 + a_1 T + a_2 S + a_3 T^2 + a_4 S^2 + a_5 T^3 + a_6 S^3 + a_7 T S + a_8 T^2 S + a_9 T S^2 \\ z_2 &= b_0 + b_1 T + b_2 S + b_3 T^2 + b_4 S^2 + b_5 T^3 + b_6 S^3 + b_7 T S + b_8 T^2 S + b_9 T S^2 \\ z_3 &= c_0 + c_1 T + c_2 S + c_3 T^2 + c_4 S^2 + c_5 T^3 + c_6 S^3 + c_7 T S + c_8 T^2 S + c_9 T S^2 \end{aligned} \tag{13}$$

BGD
11, 6461–6517, 2014

The associated coefficients are listed in Table 6, while the R program used to make these calculations, which exploits the seacarb software package for the carbonate system (Lavigne and Gattuso, 2011), is given in the Supplement. With the VAR approach applied to the range of Mediterranean temperatures (13 to 30 °C) we found that Eq. (12) fit exactly calculated values to within 0.6 % when $\delta pCO_{2_a} \leq 280$ ppm, i.e., up to a doubling of the preindustrial level of atmospheric CO_2.

For lateral boundary conditions, we restored simulated δC_T throughout the Atlantic buffer zone toward a time varying, spatially co-located section taken from the global-scale gridded derived product by Khatiwala et al. (2009) for each year between 1765 to 2011, using their values from 1800 (the start year of our anthropogenic CO_2 simulations) as our zero reference. That damping across the entire buffer zone was designed to maintain a reasonable time varying inflow of δC_T from the Atlantic across the Strait of Gibraltar.

2.3 Looping

All numerical simulations were run off-line, looping through the circulation fields from the NEMO-MED12 model. That circulation model was forced with the ARPERA forcing during 1958–2008. The first 7 years (1958–1964) are considered as a spin-up and are not used in the offline simulations of passive tracers. Rather, the next 10 years (ARPERA forcing during 1965–1974) are continuously repeated until 1975 to drive offline simulations of both passive tracers.

For both passive tracers, up until 1975, we began by looping repeatedly the same 10 years of NEMO-MED12 circulation fields, i.e., those forced by the ARPERA atmospheric forcing during 1965–1974. That forcing period was selected because it does not include intense events like the EMT or the Western Mediterranean Transition (Schroeder et al., 2008); we thus considered this period as best suited to produce reasonable circulation fields for the Mediterranean Sea (Beuvier et al., 2010, 2012b; Beuvier, 2011). Thus for the complete CFC-12 simulation, covering 1930 to 2008, the 1965–1974 loop of MED12 circulation fields was repeated 4.5 times to cover offline

BGD
11, 6461–6517, 2014

years 1930–1975 (Fig. 4). Then to complete the offline CFC-12 simulation, we applied the NEMO-MED12 circulation fields corresponding to the remaining 1975–2008 period forcing. The same 1965–1974 loop of the circulation fields from NEMO-MED12 were likewise repeated for the three anthropogenic CO_2 simulations (GLO, MED, VAR), but 17.5 times to cover offline simulation years 1800–1974. Then as for CFC-12, the last 34 years of the offline anthropogenic CO_2 simulations were piloted with the NEMO-MED12 circulation fields from the remaining 1975–2008 years of the ARPERA forcing.

2.4 δpH

The anthropogenic change in surface pH during 1800 to 2001 was computed from δC_T and prescribed total alkalinity. The preindustrial C_T was computed by assuming that the prescribed total alkalinity was in thermodynamic equilibrium with an atmospheric xCO_2 of 280 ppm at 1 atm total pressure, correcting for humidity. Computations were made with seacarb, which takes two carbonate system variables and computes all others including pH. Then to this preindustrial C_T, we added our simulated δC_T and recomputed pH. Other input variables, temperature, salinity, and total alkalinity were identical. Concentrations of phosphate and silica were assumed to be zero, a good approximation for the oligotrophic surface waters of the Mediterranean Sea. The anthropogenic change in pH is then just the difference between two computations. This exercise yields a surface map of δpH.

For deep waters, we consider changes only along one transbasin section, Meteor M51/2. Exploiting total alkalinity, C_T, temperature, and salinity measured along from this section in November 2001 (Schneider et al., 2007, 2010), we computed corresponding pH for all data points along the section and throughout the water column. Then we subsampled the simulated δC_T in 2001 at all station locations and sample depths. After removing those simulated results from the measured C_T, we recalculated pH. The difference is the δpH along the same section. For comparison, we repeated this exercise, but instead of simulated δC_T, we used the TTD data-based estimates

BGD
11, 6461–6517, 2014

of anthropogenic C_T from Schneider et al. (2010), already available along the same section.

3 Results

3.1 Evaluation

By comparing modeled to observed CFC-12, we evaluated the simulated circulation in regard to ventilation of water masses (Fig. 5). Whereas modeled CFC-12 generally matches observations between 150 m (~1.4 pmol kg^{-1}) and 1200 m (~0.3 pmol kg^{-1}), simulated concentrations do not show the observed mid-depth minimum. For instance in the Levantine sub-basin, observed CFC-12 concentrations are lowest (~0.3 pmol kg^{-1}) between 600 and 1500 m but below that depth zone concentrations grow with depth, reaching ~0.6 pmol kg^{-1} in bottom waters. Conversely, simulated concentrations below 1200 m continue to decline until they bottom out at ~0.3 pmol kg^{-1} (Fig. 6).

Generally, the model underestimates the relatively large CFC-12 concentrations observed in deep waters of the eastern and western basins (~0.6 pmol kg^{-1}), which are indicative of recently ventilated water masses (Schneider et al., 2010; Roether et al., 2007). Although the model simulates some penetration of CFC-12 south of the Crete Passage with concentrations reaching up to ~0.5 pmol kg^{-1}, those remain lower than observed. Ventilation of the model's deep eastern basin is particularly weak in the Adriatic and Ionian sub-basins (Fig. 5). On average below 2000 m, CFC-12 concentration from the model are only half of those observed. Overall, the CFC-12 evaluation indicates that the model produces an adequate ventilation of intermediate water masses but insufficient ventilation of deep waters.

BGD
11, 6461–6517, 2014

3.2 Air-sea flux

The invasion of anthropogenic carbon into the Mediterranean Sea is influenced by the δCO_2 flux at the surface and by exchange with the Atlantic Ocean across the Strait of Gibraltar. The simulated air–sea flux integrated since the beginning of the simulation (cumulative flux) is similar among the three simulations, all exhibiting maxima in the same regions (Fig. 7). The highest fluxes occur in the Gulf of Lions and to the east of Crete, both regions of deep and intermediate water formation, and in Alboran sub-basin, which is highly influenced by the strong Atlantic inflow and by the presence of 2 standing anticyclonic eddies (Vargas-Yáñez et al., 2002). Along coastlines there are local minima but also the maximum uptake at the outflow of the Dardanelles Strait although that is extremely localilzed. In the MED simulation, cumulative fluxes over the western basin are on average 25 % larger per unit area than the Mediterranean Sea's mean, whereas they are 13 % lower in the eastern basin (Table 1). Conversely, the larger surface area of the eastern basin means that its total uptake represents 58 % of the total Mediterranean Sea uptake.

The 10 % greater prescribed surface total alkalinity in the MED simulation relative to GLO means that the latter must absorb less anthropogenic carbon (Fig. 7b). Indeed, despite very similar uptake patterns, the basin-wide cumulative uptake is 17 % less in the GLO simulation than in MED, with a greater reduction in the western basin (22 %) than in the eastern basin (14 %). By definition, the salinity-derived total alkalinity in the VAR simulation is more realistic than with MED simulation, varying from 2350 µeq kg^{-1} in the Alboran sub-basin to 2650 µeq kg^{-1} in the eastern basin. That lower western total alkalinity results in an 8 % lower air–sea flux in the western basin, while the higher eastern total alkalinity drives 5 % greater uptake in the eastern basin (Fig. 7c). Yet despite these east-west differences between VAR and MED, total basin-wide uptake is only 0.3 % less in former than the latter. Overall the eastern basin always dominates, taking up 60 % of the basin-wide integrated flux in VAR and GLO and taking up 57 % in MED. However, it is not only the air–sea flux but also lateral exchange that matters.

BGD
11, 6461–6517, 2014

3.3 Budget

The Mediterranean Sea's content of anthropogenic carbon is affected not only by the air–sea flux but also by exchange with the Atlantic Ocean through the Strait of Gibraltar. To assess the relative importance of this lateral exchange we constructed a budget of δC_T in the Mediterranean Sea. In that, the temporal evolution of the cumulative air–sea flux in the reference simulation MED is compared to the same simulation's total mass of carbon that has entered and left the Mediterranean Sea through the Strait of Gibraltar (Fig. 8). The key terms are thus the flux, the net transfer at the Strait of Gibraltar (inflow – outflow of δC_T), and the actual accumulation of δC_T in the Mediterranean Sea (inventory).

In the MED simulation between 1800 and 2001, there is 1.50 Pg C that enters the Mediterranean Sea via the air–sea flux (0.78 Pg C) and via the Strait of Gibraltar inflow (0.72 Pg C) (Table 2). Yet 64 % of the δC_T inflow (by Atlantic Water near the surface) is balanced by δC_T outflow at depth (by the Mediterranean outflow). That leaves 1.04 Pg C that remains in the Mediterranean as the total δC_T inventory. Thus 25 % of the Mediterranean's total δC_T inventory is due to net exchange at the Strait of Gibraltar, while the remaining 75 % is from the air–sea flux. The budget of the VAR simulation is quite similar to that for MED, but both of those differ substantially from the budget for GLO (Table 2). In GLO, the Mediterranean Sea's δC_T inventory in 2001 (0.94 Pg C) is 10 % less, with 69 % of the total input coming from the air–sea flux and 31 % from net exchange across the Strait of Gibraltar. The evolution of the MED simulation's carbon budget (Fig. 9) demonstrates that anthropogenic carbon enters the Mediterranean entirely via the air–sea flux at the beginning of the simulation, but that the fraction entering by lateral exchange across the Strait of Gibraltar grows until stabilizing in the 1960's to one-fourth of the total.

BGD
11, 6461–6517, 2014

3.4 δC_T inventory

Having examined how anthropogenic carbon enters the Mediterranean Sea, we now turn to where it is stored, the patterns of which differ from those of the input fluxes due to water mass transport. The vertical integral of the δC_T concentration is termed the inventory. In the Mediterranean Sea, the inventory patterns tend to follow the distribution of bathymetry (Fig. 10). Thus unlike the global ocean, substantial levels of anthropogenic carbon have already penetrated into deep waters of the Mediterranean Sea, as deduced previously by observational studies (Lee et al., 2011; Schneider et al., 2010; Touratier and Goyet, 2011). Specific inventories (mass per unit area) in the reference simulation (MED) are 10 % higher in the western basin and 6 % lower in the eastern basin relative to the 33.5 mol C m^{-2} average for the Mediterranean Sea (Table 3). For the two other simulations, the basin-wide inventory is 10 % lower in GLO and 0.1 % higher in VAR. Those east-west differences are smaller than those for the air–sea flux (Table 1). There is a strong correlation between latitudinal variations in the inventory and the bathymetry, both along the METEOR M51/2 section and in terms of meridional means (Fig. 11). In both cases, the correlation is striking, except in isolated regions such as in the Ionian sub-basin (~15–20°E in Fig. 11) where poorly ventilated deep waters have relatively low δC_T concentrations.

3.5 Comparison with data-based estimates

To go beyond model comparison of simulated uptake of anthropogenic CO_2, we also compare model results to data-based estimates. In particular, we focused on data-based estimates of anthropogenic carbon deduced with TTD because that method requires only measurements of temperature, salinity, and CFC-12, all of which were simulated thereby allowing us to test the approach (see Sect. 4.1). For now though, let us simply compare model results to the TTD data-based estimates of δC_T estimated from observations collected on the METEOR M51/2 section in 2001 (Schneider et al., 2010). A first comparison reveals that the model underestimates everywhere

BGD
11, 6461–6517, 2014

the TTD data-based estimates of the inventory along the METEOR M51/2 section (Fig. 10). While the TTD inventory along this section averages 83 mol m^{-2} (ranging from 21 and 153 mol m^{-2}), the model average is 50 mol m^{-2}, 40 % less. Expanding the comparison vertically, the model is seen to underestimate the data-based estimates throughout the water column, even at the surface (Fig. 12). Surface concentrations are naturally largest, both for the TTD estimates (∼68 µmol kg^{-1}) and for the model (e.g., ∼58 µmol kg^{-1} in the MED simulation). Whereas the TTD data-based estimates are lowest (20 to 25 µmol kg^{-1}) in the Levantine sub-basin between 800 and 1500 m and increase below (e.g., reaching up to 35 µmol kg^{-1} in the EMDW), simulated δC_T decreases with depth everywhere, as already seen for simulated CFC-12 (Fig. 5). The lowest simulated δC_T concentrations are found in the bottom waters of the Ionian sub-basin (< 5 µmol kg^{-1}). However, higher deep-water δC_T is simulated in the EMDW near the Crete Passage (up to 15 µmol kg^{-1}), where there is dense-water outflow from the Aegean sub-basin through the Crete Passage, during the EMT. In terms of basin totals, Schneider et al. (2010) relied on TTD to help estimate a basin-wide anthropogenic carbon inventory of 1.7 Pg C for the Mediterranean Sea, with 1.0 Pg C of that in the Eastern basin (Table 4). Relative to the data-based estimates, the modeled basin-wide Mediterranean inventory is 40 % less in the MED and VAR and 46 % less in GLO. For the eastern inventory basin, the MED and VAR simulations are 35 % lower than the TTD data-based estimates, whereas GLO is 42 % lower.

3.6 δpH

Anthropogenic changes in surface pH between 1800 and 2001 are remarkably uniform, both between simulations and across the basin. Away from the coast, the change in surface pH between 1800 and 2001 varies between −0.078 and −0.082 in the GLO simulation (Fig. 13). Exceptions include the Northern Levantine sub-basin, where the δpH is slightly less intense (−0.076) and the more intense changes in the Gulf of Gabes, the Adriatic and Aegean sub-basins, and near the mouths of large rivers such

BGD
11, 6461–6517, 2014

as the Nile and the Rhone. The MED simulation exhibits almost identical patterns and intensities for the change in pH except in Alboran sub-basin and the western portion of the Western basin, where pH changes are less intense (−0.074 and −0.072, i.e., a difference of up to ∼0.008 pH units). Conversely, the VAR simulation with its spatially varying total alkalinity produces a more contrasted pattern of pH change. Although VAR 's spatial variability in δpH in the western basin is intermediate between that seen for GLO and MED, the eastern basin contrast in VAR is much greater. In particular, VAR 's pH changes are smallest where the salinity derived total alkalinity is highest (Levantine sub-basin), and they are largest where the salinity-derived total alkalinity is smallest (e.g., near the Po, Nile, and Dardanelles outflows). Despite differences in spatial patterns between simulations, their basin-wide average change in surface pH is almost identical -0.08 ± 0.01 units (total scale).

4 Discussion

4.1 δC_T in the Mediterranean Sea

Our comparison of modeled to measured CFC-12 indicates that the model adequately represents ventilation of near-surface and intermediate waters but underestimates ventilation of deep waters. This CFC-12 evaluation alone implies that our simulated δC_T is likewise too low in Mediterranean Sea deep waters and hence that our simulated total anthropogenic carbon inventory of 1.03 Pg C is a lower limit. Yet even in the top 400 m where there is tight agreement between simulated and observed CFC-12, the data-based estimates of δC_T from the TTD method are 20 % larger than those simulated (Fig. 6). Hence it is unlikely that the modeled circulation is the primary cause. Simplifications with the perturbation approach, e.g., its steady state assumption, could be partly to blame although errors due to circulation-induced changes in biological productivity appear small for the global ocean (Siegenthaler and Sarmiento, 1993; Sarmiento et al., 1998). Nor does the treatment of total alkalinity in the perturbation approach

BGD
11, 6461–6517, 2014

appear a significant factor, considering that our three treatments with different mean states and spatial variability give results that are quite similar (see Sect. 4.3). Besides these potential simulation biases, it is also possible that the data-based methodology, namely the TTD approach, is biased.

Hence we tested the TTD approach in the model world (MW) by (1) using it to estimate δC_T from simulated CFC-12, temperature, and salinity and (2) comparing those results to the δC_T simulated directly by the model. That comparison reveals that the TTD_{MW} estimates always overestimate the simulated δC_T. Those overestimates start at +10 % in surface waters but reach more than +100 % in Mediterranean Sea bottom waters (Fig. 14). Relative differences are highest where simulated CFC-12 is lowest, i.e., where the ventilation age of water masses are oldest, namely in bottom waters particularly those in the Ionian sub-basin. Whereas the TTD_{MW} estimate of the total anthropogenic carbon inventory in the Mediterranean Sea is 1.4 Pg C, the simulated value in the reference simulation (MED) is 1.0 Pg C. That 40 % overestimate with the TTD approach in the model world could be less in the real Mediterranean Sea, because the model underestimates CFC-12 concentrations in the deep water, which accentuates the discrepancy. Nonetheless, the TTD-based inventory of anthropogenic carbon remains an upper limit. Other data-based methods that estimate greater anthropogenic carbon inventories than TTD in the Mediterranean Sea, e.g., the TrOCA approach (Fig. 1), must overestimate the true inventory by even more. Although even the upper limit of our range (1.0 to 1.7 Pg C) is small when compared to the global ocean inventory of anthropogenic carbon of 134 Pg C (Sabine et al., 2004, for year 1994), the Mediterranean Sea contains 2.4 to 4 times as much anthropogenic carbon per unit volume as does the global ocean.

4.2 Transfer across the Strait of Gibraltar

Unlike the global ocean where outside input of anthropogenic carbon comes only from the atmosphere, in the Mediterranean Sea there is also lateral input and output of anthropogenic carbon via the Strait of Gibraltar. Unfortunately, data-based estimates of

BGD
11, 6461–6517, 2014

that net transport do not agree even in terms of its direction, much less its magnitude. That is, estimates of transport based on data-based estimates of δC_T with the TrOCA method suggest that the Mediterranean Sea is a source anthropogenic carbon to the Atlantic Ocean (Aït-Ameur and Goyet, 2006; Huertas et al., 2009); conversely, with two other data-based methods, TTD and the ΔC^* approach (Gruber et al., 1996), there is a net transport of anthropogenic carbon from the Atlantic to the Mediterranean Sea (Huertas et al., 2009; Schneider et al., 2010). The two latter back-calculation data-based methods give similar net fluxes of δC_T: ~4.2 Tg C yr^{-1} with ΔC^* and 3.5 Tg C yr^{-1} with TTD. Both rely on the estimates of water fluxes from Huertas et al. (2009) (Table 5). Both methods also produce similar estimates for the δC_T concentrations in inflowing and outflowing waters: ~60 µmol kg^{-1} in the near-surface inflowing water and ~52 µmol kg^{-1} in the deeper Mediterranean Outflow Water (MOW). However, these δC_T estimates are based on data collected from different periods, i.e., May 2005 to July 2007 for Huertas et al. (2009) and November 2001 for Schneider et al. (2010). Moreover, the transfer deduced from TTD-derived δC_T estimates from Schneider et al. are estimated to have a large uncertainty (−1.8 to 9.2 Tg C yr^{-1}). The net δC_T transfer estimated with the TrOCA method is −3 Tg C yr^{-1}. That much stronger net export from the Mediterranean Sea to the Atlantic is due to TrOCA's assessment that the outflowing MOW has higher δC_T (~80 µmol kg^{-1}) than the inflowing AW (~65 µmol kg^{-1}) (Huertas et al., 2009; Schneider et al., 2010; Flecha et al., 2011). Yet that vertical distribution is opposite to that expected from an anthropogenic transient tracer in the ocean with an atmospheric origin.

All three of our model simulations indicate a net transfer of anthropogenic carbon from the Atlantic to the Mediterranean across the Strait of Gibraltar (Sect. 3.3). In the reference simulation (MED), 0.26 Pg C enters the Mediterranean Sea via the Strait fo Gibralter between 1800 and 2001, similar to the TTD- and ΔC^*-based estimates (Table 5). Observational estimates of water transfer across the Strait of Gibraltar are between 0.72 and 1.01 Sv (1 Sverdrup (Sv) = 10^6 m^3 s^{-1}) for surface inflow and between 0.68 and 0.97 Sv for deep outflow, resulting in a net transfer of +0.04 to +0.13 Sv (Bry-

BGD
11, 6461–6517, 2014

den and Kinder, 1991; Bryden et al., 1994; Tsimplis and Bryden, 2000; Candela, 2001; Baschek et al., 2001; Lafuente et al., 2002; Soto-Navarro et al., 2010). The model falls near the lower limit of these estimates, having an inflow of 0.71 Sv, an outflow of 0.67 Sv, and a net water transfer of +0.04 Sv, when averaged between 1992 to 2008 (Beuvier, 2011). For 2005–2007, the simulated transfer is 0.15 Sv weaker than observational estimates from Huertas et al. in 2001 both for inflow and outflow, while net transfer is not significantly different: +0.04 vs. 0.05 Sv (Table 5).

Simulated δC_T concentrations in the model's AW are largely determined by damping to data-based estimates from Khatiwala et al. (2009) at the western boundary of the model domain. In the MED simulation, the δC_T in the inflowing AW is 12 to 24 % lower than data-based estimates from Huertas et al. (2009) who used both ΔC^* and TrOCA approaches (Table 5). But the largest discrepancy occurs in the outflowing deeper waters (MOW), for which the simulated δC_T underestimates the data-based ΔC^* for 2005–2007 by 31 %. That underestimate is expected given that simulated CFC-12 in the model's WMDW is only half that observed and that this deep water contributes to the MOW.

The model's underestimate of δC_T in the MOW is the determining factor which results in less outflow and thus more net inflow of anthropogenic carbon to the Mediterranean Sea. It follows that the model must provide an upper limit for the true net inflow of anthropogenic carbon, given that modeled water exchange falls within the observed range and that modeled and data-based estimates of δC_T are more similar in the inflowing water than in the outflowing water. Likewise, a lower limit for net transport of anthropogenic is offered by the computations that use data-based TTD estimates of δC_T. That follows because (1) TTD overestimates deep δC_T by more than surface values and (2) near surface inflow and deep outflow are similar in magnitude. Hence the TTD-based approach must underestimate net input of anthropogenic carbon to the Mediterranean. Therefore the net input of anthropogenic carbon across the Strait of Gibralter must be between +3.5 and +4.7 Tg C yr^{-1} based on observations collected in 2001. To compare that range to the Huertas et al.'s results for 2005–2007, we relied

BGD
11, 6461–6517, 2014

on the simulated δC_T evolution between 2001 and 2005–2007. In that 5 ± 1 year period, simulated δC_T increased by +10.5 % in the inflowing AW and by +11.2 % in the MOW. For the 2005–2007 lower limit, we applied those trends to the lower limit δC_T estimates for 2001 (Schneider et al.'s TTD estimates in the AW and MOW) combined with the 2005–2007 water transfer rates (Huertas et al., 2009); for the upper limit we again used the model result. Hence for 2005–2007, we consider that the true net input of anthropogenic carbon across the Strait of Gibraltar must fall between +3.7 and +5.5 Tg C yr^{-1}.

4.3 Sensitivity to total alkalinity

To test the sensitivity of results to total alkalinity we compared three simulations: GLO with a basin-wide total alkalinity equal to the global ocean average, MED where the basin-wide inventory is increased by 10 % (equivalent to the Mediterranean Sea's surface average), and VAR where surface total alkalinity varies as a linear function of salinity. The 10 % greater total alkalinity in MED and VAR relative to GLO results in a 10 % greater simulated inventory of anthropogenic carbon (Table 4), but the basin-integrated air–sea flux of anthropogenic in MED and VAR is 20 % greater than in GLO (Table 1). The 10 % difference must be made up by proportionally less input of anthropogenic carbon to the Mediterranean from the Atlantic in MED and VAR relative to GLO.

The MED simulation has greater total alkalinity in the western basin than either GLO or VAR and hence it absorbs more anthropogenic carbon there than do the other two simulations (Fig. 7). Yet MED 's western basin total alkalinity is too high compared to what actually comes in from the Atlantic and even in terms of the δC_T also coming in with the same water. The latter is determined in all three model runs by restoring to data-based estimates of Khatiwala et al. (2009) in the Atlantic buffer zone. Thus it is less accurate to impose a mean Mediterranean Sea total alkalinity in this area, which artificially increases the surface water buffer capacity and hence its ability to absorb CO_2. The same artefact results in a lower local change in pH (Fig. 13). Thus

BGD
11, 6461–6517, 2014

the constant Mediterranean surface total alkalinity as used in MED is suboptimal for simulating δC_T near the Strait of Gibraltar.

In contrast, the VAR simulation generally has more realistic total alkalinity that increases from west to east (Fig. 3). That avoids an over-buffered carbonate system near the Strait of Gibraltar, particularly in the Alboran sub-basin, and an under-buffered system in the far eastern Mediterranean. However, VAR is generally less realistic near river mouths than either GLO or MED. By imposing a total alkalinity that is a function of salinity in a model that considers only fresh water riverine input (no total alkalinity delivery), the model-imposed total alkalinity near river mouths is too low. That artefact results in lower air-to-sea fluxes of anthropogenic carbon when close to river mouths (Fig. 7) and locally more intense reductions in pH near the Nile, Po, and Rhone river mouths and near the outflow of the Dardanelles Strait (Fig. 13); at the latter site, the air-to-sea flux of anthropogenic carbon even changes sign from ocean uptake to loss, although that is extremely localized.

Despite these local differences, the three approaches yield similar results when integrated across the entire Mediterranean Sea, with spatial variability in total alkalinity leading to differences in global inventory of only 0.1 % and differences between east-west partitioning of less than 1 %.

4.4 Change in pH

Two recent studies have attempted to quantify the decline in the pH of the Mediterranean Sea due to the increase in anthropogenic carbon (Touratier and Goyet, 2009, 2011). Both concluded that the pH reduction in the Mediterranean Sea (acidification), is larger than that experienced by typical waters of the global ocean. The higher total alkalinity of the Mediterranean Sea was evoked to justify a larger uptake of anthropogenic carbon. Our results support that finding, i.e., with the MED – GLO showing a 10 % increase in anthropogenic carbon inventory that occurs when average surface total alkalinity is increased by 10 % (Mediterranean minus global ocean average).

BGD
11, 6461–6517, 2014

The same two studies further suggest that higher levels of δC_T in the Mediterranean Sea also imply greater changes in pH. Yet our sensitivity tests demonstrate that the higher total alkalinity of the Mediterranean Sea does not result in a greater anthropogenic reduction in surface pH. Differences between simulations GLO and MED are negligible (Fig. 13). In both, the simulated decline in surface pH is −0.08 units when averaged across Mediterranean Sea. Hence the decline in pH is quite similar between typical surface waters in the Mediterranean Sea and those in the global ocean.

For clearer illustration, let us compare these findings from an ocean model, where oceanic and atmospheric CO_2 are not in equilibrium, with calculations that assume thermodynamic equilibrium. By imposing the same atmospheric CO_2 increase (from 280 to 450 ppm) to be in equilibrium with surface water at three different alkalinities (2300, 2450 and 2600 µmol kg^{-1}), we can for each total alkalinity compute corresponding changes in all other carbonate system variables, including C_T and pH (Fig. 15).

At the beginning (280 ppm), the higher total alkalinity produces higher calculated C_T and higher calculated pH. At each total alkalinity, as atmospheric CO_2 increases, calculated C_T increases and calculated pH decreases. The same change in atmospheric CO_2 from 280 to 450 ppm produces larger changes in calculated C_T when total alkalinity is larger (e.g., a 14 % greater increase with a total alkalinity of 2600 instead of 2300 µmol kg^{-1}). Conversely, corresponding changes in pH differ by less than 1 %. This simple equilibrium calculation confirms our ocean model results as well as results from a previous study (Orr, 2011, Fig. 3.6). Although the higher total alkalinity of the Mediterranean Sea enhances its anthropogenic carbon content by 10 %, the anthropogenic reduction in surface pH is not significantly different from that for typical surface waters of the global ocean.

Anthropogenic carbon is already present in substantial quantities throughout the water column of the Mediterranean Sea (Fig. 12). Hence the anthropogenic decline in pH also affects the entire water column. Touratier and Goyet (2011) found that the anthropogenic pH change in some Mediterranean bottom waters has already reached values of up to −0.12, higher even than at the surface. However, they deduce those

BGD
11, 6461–6517, 2014

high values from data-based estimates of δC_T using the TrOCA approach, which overestimates actual values, particularly at depth (see Sects. 1 and 4.1). To estimate subsurface anthropogenic changes in pH, we used a simple 3-step method: (1) we relied on discrete measurements of C_T, total alkalinity, and phosphate and silicate concentrations on the 2001 Meteor M51/2 cruise to compute a modern reference pH using seacarb; (2) we subsampled the MED model at the same time, positions, and depths to get corresponding simulated δC_T; and (3) we subtracted the latter from the modern measurements of C_T to get preindustrial C_T, using that along with the measured values of other input variables (assuming they had not changed) to compute a preindustrial pH. We then compared that model-derived change in pH (δpH_{model}) to the data-based TTD estimates (δpH_{TTD}) calculated in the same fashion, i.e., using TTD δC_T instead of modeled δC_T in the computation sequence (Fig. 16). The resulting anthropogenic change in surface pH ranges from −0.08 to −0.10 units. Below the surface, δpH_{model} gradually becomes less intense until reaching the bottom where it ranges from −0.005 pH units in the Ionian sub-basin to −0.03 in the Crete Passage. Those changes must be underestimates given the model's poor ventilation of deep waters based on the CFC-12 evaluation (Sect. 3.1). The data-based change in δpH_{TTD} exhibits its weakest magnitude (−0.035 pH units) between 1000 and 1500 m in the Levantine sub-basin, where the TTD data-based δC_T is at a minimum. Deeper down, δpH_{TTD} increases in magnitude, reaching up to −0.06 pH units in the bottom waters of the Ionian sub-basin.

As the model results and the TTD data-based approach provide lower and upper limits for the actual changes in deep-water δC_T, it follows that they also provide bounds for the anthropogenic change in pH. The actual change in bottom water pH in the eastern basin thus lies between −0.005 and −0.06 units.

5 Conclusions

A first simulation of anthropogenic carbon in the Mediterranean Sea suggests that it accumulated 1.0 Pg C between 1800 and 2001. That estimate provides a lower limit

BGD
11, 6461–6517, 2014

based on comparison of observed vs. simulated CFC-12 in the same model, which reveals that modeled deep waters are poorly ventilated. Furthermore, we demonstrate that a previous data-based estimate of 1.7 Pg C (Schneider et al., 2010) is an upper limit after testing the associated TTD approach in our model. In 2001 in the reference model, a total of 1.5 Pg C of anthropogenic carbon had entered the Mediterranean Sea with 52 % from the air–sea flux and 48 % from Atlantic Water inflow; however, 31 % of that total had also left via the deep Mediterranean Outflow Water. Out of the net accumulation of 1.0 Pg C, 75 % comes from the air-to-sea flux and 25 % from net transfer across the Strait of Gibraltar. The rate of net exchange across that strait to the Mediterranean is from 3.5 to 4.7 Tg C yr^{-1} in 2001 and from 3.7 to 5.5 Tg C yr^{-1} in 2005–2007, based on the model and TTD results.

Our estimates of anthropogenic carbon also allow us to assess anthropogenic changes in pH. Although the 10 % higher mean total alkalinity of the Mediterranean Sea is responsible for a 10 % increase in anthropogenic carbon inventory, that does not significantly affect the anthropogenic change in surface pH. That average surface pH change −0.08 units for both the Mediterranean Sea and the global ocean. In contrast, relative to the global ocean, Mediterranean deep waters exhibit a larger anthropopogenic change in pH because their ventilation times are faster. In 2001, the δpH in Mediterranean Sea bottom waters is estimated to lie between −0.005 to −0.06 units based on our limits from simulated and TTD data-based δC_T. These findings do not support previous conclusions that the anthropogenic change in the pH of Mediterranean deep waters is as high as −0.12 units, which is more intense even than the surface change (Touratier and Goyet, 2009, 2011). Furthermore those previous findings rely on the TrOCA data-based estimates of δC_T, which are much larger than the TTD data-based estimates, shown in Sect. 4.1 to be already an upper limit.

Future studies that include the full natural carbon cycle and the effects of climate change are needed to confirm these results and predict future changes while weighing geochemical vs. climate factors. Improved assessment of local changes along coastlines will require improved boundary conditions, particularly for riverine and groundwa-

BGD
11, 6461–6517, 2014

ter discharge of nutrients, carbon, and total alkalinity, combined with developments to improve coastal aspects of the physical and biogeochemical models.

Supplementary material related to this article is available online at http://www.biogeosciences-discuss.net/11/6461/2014/bgd-11-6461-2014-supplement.zip.

Acknowledgements. We thank Samar Khatiwala for providing his data-based estimates for anthropogenic carbon, which we used as a lateral boundary condition for the Atlantic portion of our model domain. We thank Météo-France/CNRM and in particular Michel Déqué and Florence Sevault for running and providing the ARPERA dataset. This work was supported by the French SiMED project (Mercator Ocean), the MORCE and MED-ICCBIO projects (GIS), and the EU FP7 project MedSeA (grant 265103). This work is a contribution to the HyMeX and MERMEX programmes, and it was granted access to the HPC resources of IDRIS (Institut du Développement et des Ressources en Informatique Scientifique) of the Centre National de la Recherche Scientifique (CNRS) under allocations for years 2010, 2011 and 2012 (project 1010227) made by Grand Equipement National de Calcul Intensif (GENCI).

References

Aït-Ameur, N. and Goyet, C.: Distribution and transport of natural and anthropogenic CO_2 in the Gulf of Cádiz, Deep-Sea Res. Pt. II, 53, 1329–1343, 2006. 6463, 6482, 6500

Antonov, J. I., Locarnini, R. A., Boyer, T. P., Mishonov, A. V., and Garcia, H. E.: World Ocean Atlas 2005, vol. 2: Salinity, edited by: Levitus, S., NOAA Atlas NESDIS 62, US Government Printing Office, Washington DC, 182 pp., 2006. 6466

Attané, I. and Courbage, Y.: La démographie en Méditerranée, Situation et projections, Economica – Plan Bleu, 2001. 6462

Attané, I. and Courbage, Y.: Demography in the Mediterranean region: situation and projections, Plan Bleu, 2004. 6462

Baschek, B., Send, U., Lafuente, J. G., and Candela, J.: Transport estimates in the Strait of Gibraltar with a tidal inverse model, J. Geophys. Res., 106, 31033–31, 2001. 6483

BGD
11, 6461–6517, 2014

Béranger, K., Mortier, L., and Crépon, M.: Seasonal variability of water transport through the Straits of Gibraltar, Sicily and Corsica, derived from a high-resolution model of the Mediterranean circulation, Prog. Oceanogr., 66, 341–364, 2005. 6466

Beuvier, J.: Modélisation de la variabilité climatique et des masses d'eau en mer Méditerranée: impact des échanges océan-atmosphère, Ph. D. thesis, Ecole Polytechnique, Palaiseau, France, 2011. 6473, 6483

Beuvier, J., Sevault, F., Herrmann, M., Kontoyiannis, H., Ludwig, W., Rixen, M., Stanev, E., Béranger, K., and Somot, S.: Modelling the Mediterranean Sea interannual variability over the last 40 years: focus on the EMT, J. Geophys. Res., 115, C08017, doi:10.1029/2009JC005950, 2010. 6466, 6467, 6473

Beuvier, J., Béranger, K., Lebeaupin Brossier, C., Somot, S., Sevault, F., Drillet, Y., Bourdallé-Badie, R., Ferry, N., and Lyard, F.: Spreading of the Western Mediterranean Deep Water after winter 2005: Time scales and deep cyclone transport, J. Geophys. Res., 117, C07022 doi:10.1029/2011JC007679, 2012a. 6465, 6466

Beuvier, J., Lebeaupin Brossier, C., Béranger, K., Arsouze, T., Bourdallé-Badie, R., Deltel, C., Drillet, Y., Drobinski, P., Lyard, F., Ferry, N., Sevault, F., and Somot, S.: MED12, Oceanic component for the modelling of the regional Mediterranean Earth System, Mercator Ocean Quarterly Newsletter, 46, 60–66, 2012b. 6466, 6467, 6473

Bryden, H. L. and Kinder, T. H.: Steady two-layer exchange through the Strait of Gibraltar, Deep-Sea Res. Pt. I, 38, S445–S463, 1991. 6482

Bryden, H. L., Candela, J., and Kinder, T. H.: Exchange through the Strait of Gibraltar, Prog. Oceanogr., 33, 201–248, 1994. 6483

Candela, J.: Mediterranean Water and Global Circulation, vol. 77, Elsevier, 419 pp., 2001. 6483

Daget, N., Weaver, A., and Balmaseda, M.: Ensemble estimation of background-error variances in a three-dimensional variational data assimilation system for the global ocean, Q. J. Roy. Meteor. Soc., 135, 1071–1094, 2009. 6466

Diffenbaugh, N. S. and Giorgi, F.: Climate change hotspots in the CMIP5 global climate model ensemble, Climatic Change, 114, 813–822, 2012. 6462

Dutay, J.-C., Bullister, J. L., Doney, S. C., Orr, J. C., Najjar, R., Caldeira, K., Campin, J.-M., Drange, H., Follows, M., Gao, Y., Gruber, N., Hecht, M. W., Ishida, A., Joos, F., Lindsay, K., Madec, G., Maier-Reimer, E., Marshall, J. C., Matear, R. J., Monfray, P., Mouchet, A., Plattner, G.-K., Sarmiento, J., Schlitzer, R., Slater, R., Totterdell, I. J., Weirig, M.-F., Yamanaka, Y.

BGD
11, 6461–6517, 2014

and Yool, A.: Evaluation of ocean model ventilation with CFC-11: comparison of 13 global ocean models, Ocean Model., 4, 89–120, 2002. 6468
El Boukary, M. M. S.: Impact des activités humaines sur les cycles biogéochimiques en mer Méditerranée, Ph. D. thesis, Unniversité Paris VI - Pierre et Marie Curie, 2005. 6463
Enting, I. G., Wigley, T. M. L., and Heimann, M.: Future emissions and concentrations of carbon dioxide: key ocean/atmosphere/land analyses, Tech. pap. 31, Div. of Atmos. Res., Commonw. Sci., and Ind. Res. Org., Melbourne, Australia, 1994. 6469
Ferry, N., Parent, L., Garric, G., Barnier, B., Jourdain, N. C., and the Mercator-Ocean-team: Mercator global eddy permitting ocean reanalysis GLORYS1V1: description and results, Merc. Oc. Quart. Newsletter, 36, 15–28, 2010. 6466
Flecha, S., Pérez, F. F., Navarro, G., Ruiz, J., Olivé, I., Rodríguez-Gálvez, S., Costas, E., and Huertas, I. E.: Anthropogenic carbon inventory in the Gulf of Cádiz, J. Marine Syst., 92, 67–75, 2011. 6463, 6482
Gibelin, A.-L., and Déqué, M.: Anthropogenic climate change over the Mediterranean region simulated by a global variable resolution model, Clim. Dynam., 20, 327–339, 2003. 6462
Giorgi, F.: Climate change hot-spots, Geophys. Res. Lett., 33, L08707, doi:10.1029/2006GL025734, 2006. 6462
Giorgi, F. and Lionello, P.: Climate change projections for the Mediterranean region, Glob. Planet. Change, 63, 90–104, doi:10.1016/j.gloplacha.2007.09.005, 2008. 6462
GLOBALVIEW–CO_2: Cooperative Atmospheric Data Integration Project – Carbon Dioxide, NOAA ESRL, Boulder, Colorado, available at: http://www.esrl.noaa.gov/gmd/ccgg/globalview, 2010. 6470
Gruber, N., Sarmiento, J. L., and Stocker, T. F.: An improved method to detect anthropogenic CO_2 in the oceans., Global Biogeochem. Cy., 10, 809–837, 1996. 6482
Herrmann, M. and Somot, S.: Relevance of ERA40 dynamical downscaling for modeling deep convection in the Mediterranean Sea, Geophys. Res. Lett., 35, L04607, doi:10.1029/2007GL032442, 2008. 6466
Herrmann, M., Somot, S., Sevault, F., Estournel, C., and Déqué, M.: Modeling the deep convection in the northwestern Mediterranean Sea using an eddy-permitting and an eddy-resolving model: Case study of winter 1986–1987, J. Geophys. Res., 113, C04011, doi:10.1029/2006JC003991, 2008. 6467

BGD
11, 6461–6517, 2014

Herrmann, M., Sevault, F., Beuvier, J., and Somot, S.: What induced the exceptional 2005 convection event in the Northwestern Mediterranean basin? Answers from a modeling study., J. Geophys. Res., 115, C12051, doi:10.1029/2010JC006162, 2010. 6466

Huertas, I. E., Ríos, A. F., García-Lafuente, J., Makaoui, A., Rodríguez-Gálvez, S., Sánchez-Román, A., Orbi, A., Ruíz, J., and Pérez, F. F.: Anthropogenic and natural CO_2 exchange through the Strait of Gibraltar, Biogeosciences, 6, 647–662, doi:10.5194/bg-6-647-2009, 2009. 6463, 6482, 6483, 6484, 6500

Key, R. M., Sabine., C. L., Lee, K., Wanninkhof, R., Bullister, J., Feely, R. A., Millero, F. J., Mordy, C., and Peng, T.-H.: A global ocean carbon climatology: results from Global Data Analysis Project (GLODAP), Global Biogeochem. Cy., 18, GB4031, doi:10.1029/2004GB002247, 2004. 6472

Khatiwala, S., Primeau, F., and Hall, T.: Reconstruction of the history of anthropogenic CO_2 concentrations in the ocean, Nature, 462, 346–349, doi:10.1038/nature08526, 2009. 6473, 6483, 6484

Lachkar, Z., Orr, J. C., Dutay, J.-C., and Delecluse, P.: Effects of mesoscale eddies on global ocean distributions of CFC-11, CO_2, and $\Delta^{14}C$, Ocean Sci., 3, 461–482, doi:10.5194/os-3-461-2007, 2007. 6470

Lafuente, J. G., Delgado, J., Vargas, J. M., Vargas, M., Plaza, F., and Sarhan, T.: Low-frequency variability of the exchanged flows through the Strait of Gibraltar during CANIGO, Deep-Sea Res. Pt. II, 49, 4051–4067, 2002. 6483

Lavigne, H. and Gattuso, J.-P.: seacarb: seawater carbonate chemistry with R. R package version 2.4, available at: http://CRAN.R-project.org/package=seacarb, 2011. 6473, 6516

Lebeaupin Brossier, C., Béranger, K., Deltel, C., and Drobinski, P.: The Mediterranean response to different space-time resolution atmospheric forcings using perpetual mode sensitivity simulations, Ocean Model., 36, 1–25, doi:10.1016/j.ocemod.2010.10.008, 2011. 6465

Lee, K., Sabine, C. L., Tanhua, T., Kim, T.-W., Feely, R. A., and Kim, H.-C.: Roles of marginal seas in absorbing and storing fossil fuel CO_2, Energy Environ. Sci., 4, 1133–1146, doi:10.1039/C0EE00663G, 2011. 6478

Locarnini, R. A., Mishonov, A. V., Antonov, J. I., Boyer, T. P., and Garcia, H. E.: World Ocean Atlas 2005, Volume 1: Temperature, S. Levitus, Ed., NOAA Atlas NESDIS 61, US Government Printing Office, Washington, D. C., 182 pp., 2006. 6466

Ludwig, W., Dumont, E., Meybeck, M., and Heussner, S.: River discharges of water and nutrients to the Mediterranean and Black Sea: Major drivers for ecosystem changes during past

BGD
11, 6461–6517, 2014

and future decades?, Prog. Oceanogr., 80, 199–217, doi:10.1016/j.pocean.2009.02.001, 2009. 6466
Madec, G. and The-NEMO-Team: NEMO ocean engine, Note du pole de modélisation de l'IPSL no. 27, Institut Pierre Simon Laplace, ISSN No. 1228–1619, 2008. 6465
Orr, J. C.: Recent and future changes in ocean carbonate chemistry, in: Ocean Acidification, edited by: Gattuso, J. and Hansson, L., Oxford University press, Oxford, 41–66, 2011. 6486
Roether, W., Manca, B., Klein, B., Bregant, D., Georgopoulos, D., Beitzel, V., Kovacevic, V., and Luchetta, V.: Recent changes in eastern Mediterranean deep waters, Science, 271, 333–335, doi:10.1126/science.271.5247.333, 1996. 6467
Roether, W., Klein, B., Manca, B. B., Theocharis, A., and Kioroglou, S.: Transient Eastern Mediterranean deep waters in response to the massive dense-water output of the Aegean Sea in the 1990s, Prog. Oceanogr., 74, 540–571, doi:10.1016/j.pocean.2007.03.001, 2007. 6467, 6475
Sabine, C. L., Feely, R. A., Gruber, N., Key, R. M., Lee, K., Bullister, J. L., Wanninkhof, R., Wong, C. S., Wallace, D. W. R., Tilbrook, B., Millero, F. J., Peng, T.-H., Kozyr, A., Ono, T., and Rios, A.: The ocean sink for anthropogenic CO_2, Science, 305, 367–370, doi:10.1126/science.1097403, 2004. 6481
Sarmiento, J. L., Orr, J. C., and Siegenthaler, U.: A perturbation simulation of uptake in an ocean general circulation model, J. Geophys. Res., 97, 3621–3645, 1992. 6464, 6469, 6470, 6471
Sarmiento, J. L., Hughes, T. M., Stouffer, R. J., and Manabe, S.: Simulated response of the ocean carbon cycle to anthropogenic climate warming, Nature, 393, 245–249, 1998. 6480
Schneider, A., Wallace, D. W. R., and Körtzinger, A.: Alkalinity of the Mediterranean Sea, Geophys. Res. Lett., 34, L15608, doi:10.1029/2006GL028842, 2007. 6472, 6474, 6504
Schneider, A., Tanhua, T., Körtzinger, A., and Wallace, D. W. R.: High anthropogenic carbon content in the eastern Mediterranean, J. Geophys. Res., 115, C12050, doi:10.1029/2010JC006171, 2010. 6463, 6474, 6475, 6478, 6479, 6482, 6488, 6499, 6500, 6502, 6507, 6511, 6517
Schroeder, K., Ribotti, A., Borghini, M., Sorgente, R., Perilli, A., and Gasparini, G.: An extensive western Mediterranean deep water renewal between 2004 and 2006, Geophys. Res. Lett., 35, L18605, doi:10.1029/2008GL035146, 2008. 6473
Siegenthaler, U. and Joos, F.: Use of a simple model for studying oceanic tracer distributions and the global carbon cycle, Tellus B, 44, 186–207, 1992. 6469

BGD
11, 6461–6517, 2014

Siegenthaler, U. and Sarmiento, J.: Atmospheric carbon dioxide and the ocean, Nature, 365, 119–125, 1993. 6480

Somot, S., Sevault, F., and Déqué, M.: Transient climate change scenario simulation of the Mediterranean Sea for the 21st century using a high-resolution ocean circulation model., Clim. Dynam., 27, 851–879, doi:10.1007/s00382-006-0167-z, 2006. 6466

Soto-Navarro, J., Criado-Aldeanueva, F., García-Lafuente, J., and Sánchez-Román, A.: Estimation of the Atlantic inflow through the Strait of Gibraltar from climatological and in situ data, J. Geophys. Res., 115, C10023, doi:10.1029/2010JC006302, 2010. 6483

Soto-Navarro, J., Somot, S., Sevault, F., Beuvier, J., Béranger, K., Criado-Aldeanueva, F., and García-Lafuente, J.: Evaluation of regional ocean circulation models for the Mediterranean Sea at the strait of Gibraltar: volume transport and thermohaline properties of the outflow, Clim. Dynam., in revision, 2014. 6466

Stanev, E. V. and Peneva, L.: Regional sea level response to global climatic change: Black Sea examples, Global Planet. Change, 32, 33–47, 2002. 6466

The MerMEX group: Marine ecosystems' responses to climatic and anthropogenic forcings in the Mediterranean, Prog. Oceanogr., 91, 97–166, doi:10.1016/j.pocean.2011.02.003, 2011. 6462

Touratier, F. and Goyet, C.: Decadal evolution of anthropogenic CO_2 in the northwestern Mediterranean Sea from the mid-1990s to the mid-2000s, Deep-Sea Res. Pt. I, 56, 1708–1716, 2009. 6463, 6485, 6488

Touratier, F. and Goyet, C.: Impact of the Eastern Mediterranean Transient on the distribution of anthropogenic CO_2 and first estimate of acidification for the Mediterranean Sea, Deep-Sea Res. Pt. I, 58, 1–15, doi:10.1016/j.dsr.2010.10.002, 2011. 6463, 6478, 6485, 6486, 6488, 6502

Touratier, F., Azouzi, L., and Goyet, C.: CFC-11, $\delta^{14}C$ and ^{3}H tracers as a means to asses anthropogenic CO_2 concentrations in the ocean, Tellus B, 59, 318–325, 2007. 6463

Tsimplis, M. and Bryden, H.: Estimation of the transports through the Strait of Gibraltar, Deep-Sea Res. Pt. I, 47, 2219–2242, 2000. 6483

Vargas-Yáñez, M., Plaza, F., Garcıa-Lafuente, J., Sarhan, T., Vargas, J., and Velez-Belchi, P.: About the seasonal variability of the Alboran Sea circulation, J. Marine Syst., 35, 229–248, 2002. 6476

BGD
11, 6461–6517, 2014

Vörösmarty, C. J., Fekete, B. M., and Tucker, B. A.: Global River Discharge Database (RivDIS V1.0), International Hydrological Program, Global Hydrological Archive and Analysis Systems, UNESCO, Paris, 1996. 6466

Wanninkhof, R.: Relationship between wind speed and gas exchange over the ocean, J. Geophys. Res., 97, 7373–7382, 1992. 6468, 6469, 6470

Warner, M. J. and Weiss, R. F.: Solubilities of chlorofluorocarbons 11 and 12 in water and seawater, Deep-Sea Res. Pt. I, 32, 1485–1497, 1985. 6468

Waugh, D. W., Hall, T. M., McNeil, B. I., Key, R., and Matear, R. J.: Anthropogenic CO_2 in the oceans estimated using transit time distributions, Tellus B., 58, 376–389, 2006. 6463

Weiss, R. F.: Carbon dioxide in water and seawater: the solubility of a non-ideal gas, Mar. Chem., 2, 203–215, 1974. 6470

BGD
11, 6461–6517, 2014

Table 1. Cumulative flux between 1800 and 2001 for the three simulations, given in mol C m^{-2} and in Pg C for the Eastern and Western basins and for the entire Mediterranean Sea.

	Average flux (mol C m^{-2})			Total flux (Pg C)		
	East	West	Med Sea	East	West	Med Sea
GLO	19.2	24.8	21.0	0.39	0.26	0.65
MED	22.3	31.8	25.5	0.45	0.33	0.78
VAR	23.4	29.4	25.4	0.47	0.31	0.78

BGD
11, 6461–6517, 2014

Table 2. Budget of the anthropogenic carbon accumulated in the Mediterranean Sea (Pg C) between 1800 and 2001. The budget distinguishes Strait of Gibralter inflow ($G - S_{In}$) via the AW, the corresponding outflow ($G - S_{Out}$) via the MOW, and the air–sea flux (air–sea). Critical combined terms are thus the net inflow-outflow difference (Net $G - S$), the Total Input ($G - S_{In}$ + air–sea), and the Net Total (Net $G - S$ + air–sea).

Simulation	$G - S_{In}$	$G - S_{Out}$	Net $G - S$	air–sea	Total Input	Net Total
GLO	0.71	0.42	0.29	0.65	1.36	0.94
MED	0.72	0.46	0.26	0.78	1.5	1.04
VAR	0.72	0.46	0.26	0.78	1.5	1.04

BGD
11, 6461–6517, 2014

Table 3. Average δC_T inventories (mol C m^{-2}) in the eastern and western basins and for the entire Mediterranean Sea.

Simulation	Average inventory (mol C m^{-2}) East	West	Med Sea
GLO	28.6	33.4	30.2
MED	31.8	36.9	33.5
VAR	32.0	36.6	33.6

BGD
11, 6461–6517, 2014

Table 4. Total δC_T inventory (Pg C) for the entire Mediterranean Sea and for just the Eastern basin as simulated and as estimated by the TTD data-based method (Schneider et al., 2010).

Approach	Med Sea	East
GLO model	0.93	0.58
MED model	1.03	0.65
VAR model	1.03	0.65
TTD data	1.7 (1.3–2.1)	1.0 (0.7–1.2)

BGD
11, 6461–6517, 2014

Table 5. Lateral fluxes of water and anthropogenic carbon across the Strait of Gibraltar.

Approach	Year(s)	Net fluxes[7] ($Tg\,C\,yr^{-1}$)	Q_{in} (Sv)	$\delta C_{T;in}$ ($\mu mol\,kg^{-1}$)	Q_{out} (Sv)	$\delta C_{T;out}$ ($\mu mol\,kg^{-1}$)
(ΔC^*)[1,2]	2005–2007	$+4.20 \pm 0.04$	0.89	60	0.85	51
(ΔC^*)[1,3]	2005–2007		0.85	61	0.81	52
(TrOCA)[1,2]	2005–2007	-3.00 ± 0.04	0.89	64	0.85	78
(TrOCA)[1,3]	2005–2007		0.85	69	0.81	81
(TTD)[4]	2001	+3.5 (−1.8 to 9.2)	0.89[5]	62.4[6]	0.85[5]	54.8
Model MED	2001	+4.7	0.70	47.6	0.66	32.1
Model MED	2005–2007	+5.5	0.74	52.6	0.69	35.7

[1] Huertas et al. (2009) estimates based on data near the Strait of Gibraltar during 2005–2007.
[2] method applied to observations on the Atlantic side of the Strait of Gibraltar.
[3] method applied to observations on the Mediterranean side of the Strait of Gibraltar during May 2005 to Jul 2007.
[4] Schneider et al. (2010) estimates using the TTD approach with observations from 2001.
[5] Schneider et al.'s water fluxes across the Strait of Gibralter are from Huertas et al. (2009).
[6] Schneider et al.'s δC_T concentration in inflowing AW is from Aït-Ameur and Goyet (2006).
[7] Positive values indicate transfer from the Atlantic to the Mediterranean Sea.

BGD
11, 6461–6517, 2014

Table 6. Coefficients a_i, b_i, and c_i (where the index i varies from 0 to 9) used to compute z_1, z_2, and z_3 with Eq. (13).

i	a_i	b_i	c_i
0	1.177825e+1	9.330105e−2	1.350359e−3
1	−1.614090e−1	−1.857070e−3	−2.422081e−5
2	−5.633789e−1	−5.251668e−3	−8.087972e−5
3	1.102070e−3	1.615968e−5	1.558226e−7
4	1.027733e−2	1.028834e−4	1.655765e−6
5	−4.195387e−6	−5.816404e−8	−3.503140e−10
6	−6.677595e−5	−6.915741e−7	−1.151323e−8
7	5.292828e−3	6.857606e−5	9.547726e−7
8	−1.529681e−5	−2.836387e−7	−3.012886e−9
9	−4.737909e−5	−6.551447e−7	−9.651931e−9

BGD
11, 6461–6517, 2014

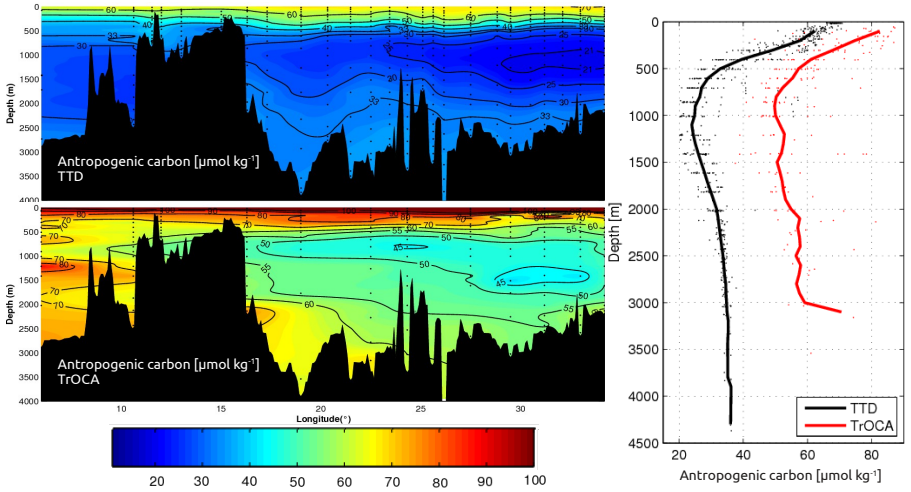

Fig. 1. Anthropogenic carbon ($\mu mol\,kg^{-1}$) estimated with two data-based methods, TTD (Schneider et al., 2010) and TrOCA (Touratier and Goyet, 2011), along the METEOR M51/2 section (November 2001). Vertical profiles on the right are for mean anthropogenic C_T along the section estimated by each method.

BGD
11, 6461–6517, 2014

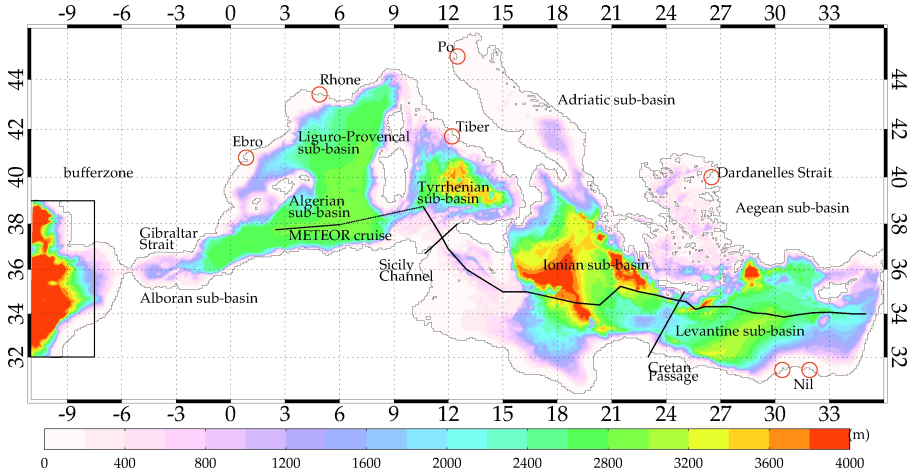

Fig. 2. Map of the MED12 model domain and bathymetry with location of the main Mediterranean sub-basins (s-b): Adriatic, Aegean, Alboran, Algerian, Liguro-Provençal, Ionian, Levantine, and Tyrrhenian. Red circles indicate the mouths of the main Mediterranean rivers (Ebro, Rhone, Tiber, Po, and Nile) and the input from the Black Sea at the Dardanelles strait. Black lines indicate the Sicily channel, the Crete Passage, and the trans-Mediterranean section from the METEOR M51/2 cruise (november 2001). The rectangular area in the western part of the model domain indicates the Atlantic bufferzone (see Sects. 2.1 and 2.2.2). The eastern basin is situated to the east of the Sicily Channel, while the western basin is situated between the Strait of Gibraltar and the Sicily Channel. The entire Mediterranean Sea refers to all waters east of the Strait of Gibraltar.

BGD
11, 6461–6517, 2014

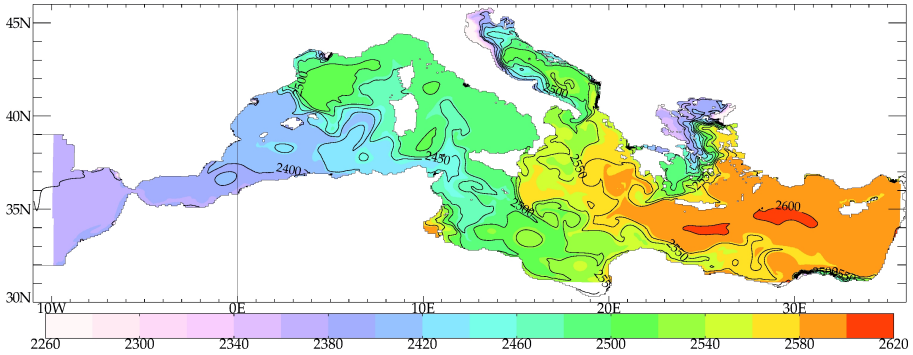

Fig. 3. Salinity-derived surface total alkalinity field ($\mu mol\,kg^{-1}$) calculated with Schneider et al.'s (2007) formula (Eq. 11) applied to the model's surface salinity field from November 2001.

BGD
11, 6461–6517, 2014

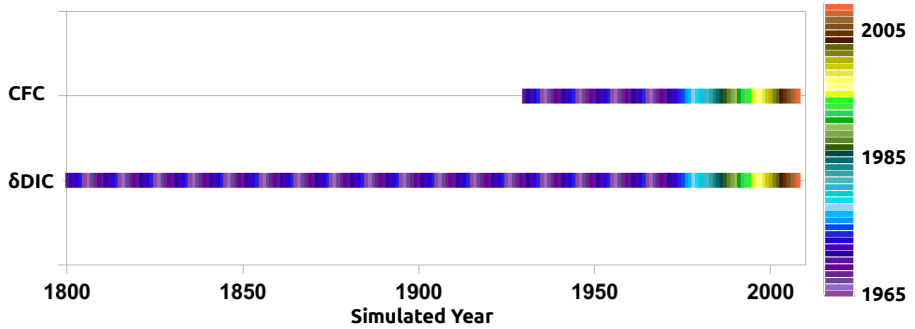

Fig. 4. Looping of dynamical atmospheric forcing fields for our CFC-12 and δC_T simulations. Colors indicate the year of the forcing.

BGD
11, 6461–6517, 2014

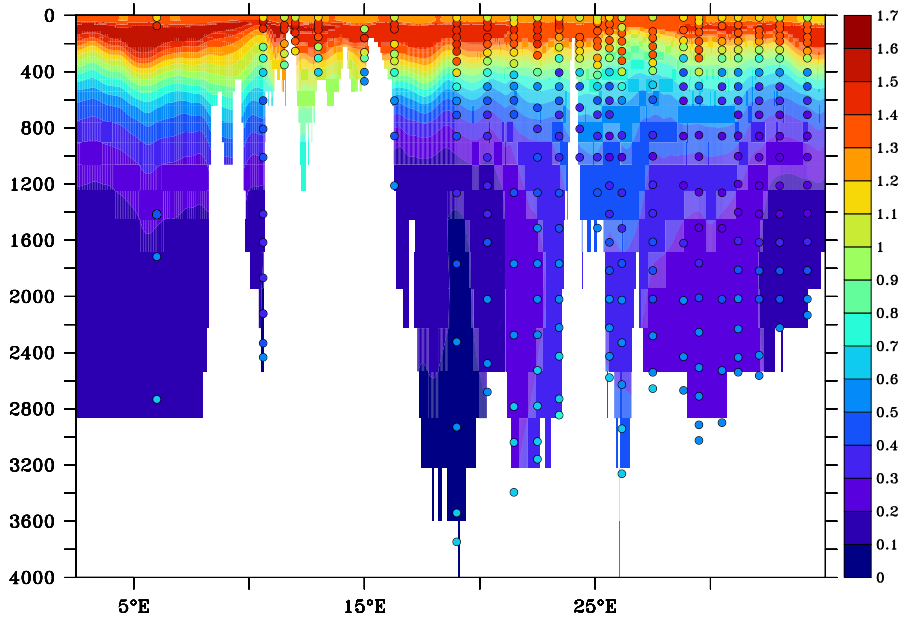

Fig. 5. CFC-12 (pmol kg^{-1}) data-model comparison along the METEOR M51/2 section. Color-filled contours indicate simulated CFC-12, whereas color-filled dots show in-situ observations. Both use the same color scale and are taken at the same time (November 2001).

BGD
11, 6461–6517, 2014

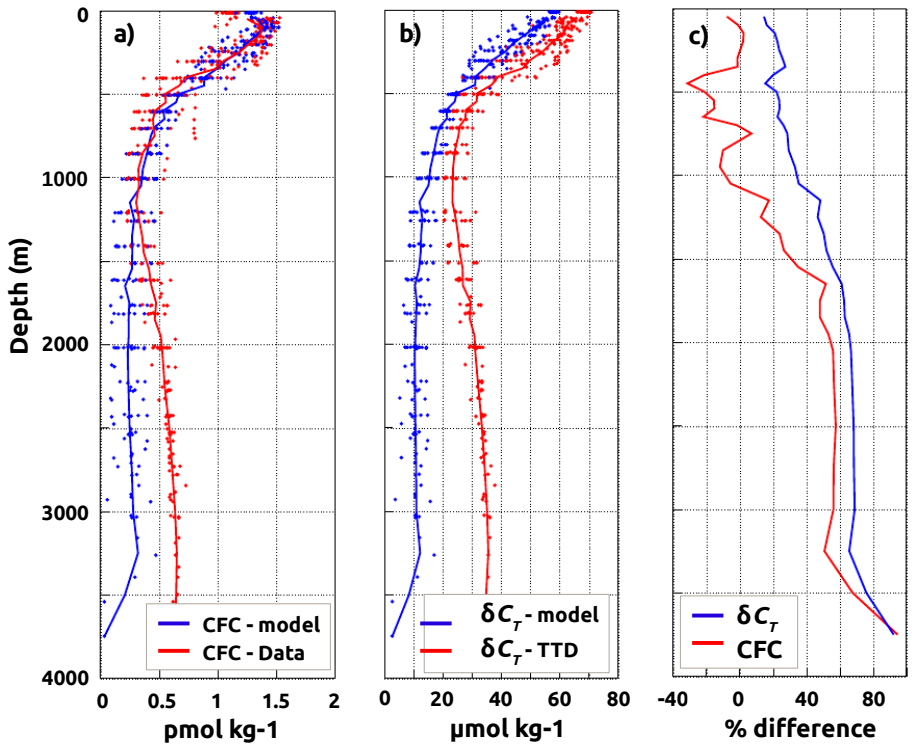

Fig. 6. Comparison of average vertical profiles along the METEOR M51/2 section for **(a)** CFC-12 (pmol kg^{-1}), **(b)** δC_T (μmol kg^{-1}), and **(c)** the model-data relative difference (in percent). Model results are in blue, while red indicates the CFC-12 data and δC_T data-based estimates; the right panel **(c)** uses blue for δC_T and red for CFC-12. Data-based estimates for δC_T are the TTD results from Schneider et al. (2010).

BGD
11, 6461–6517, 2014

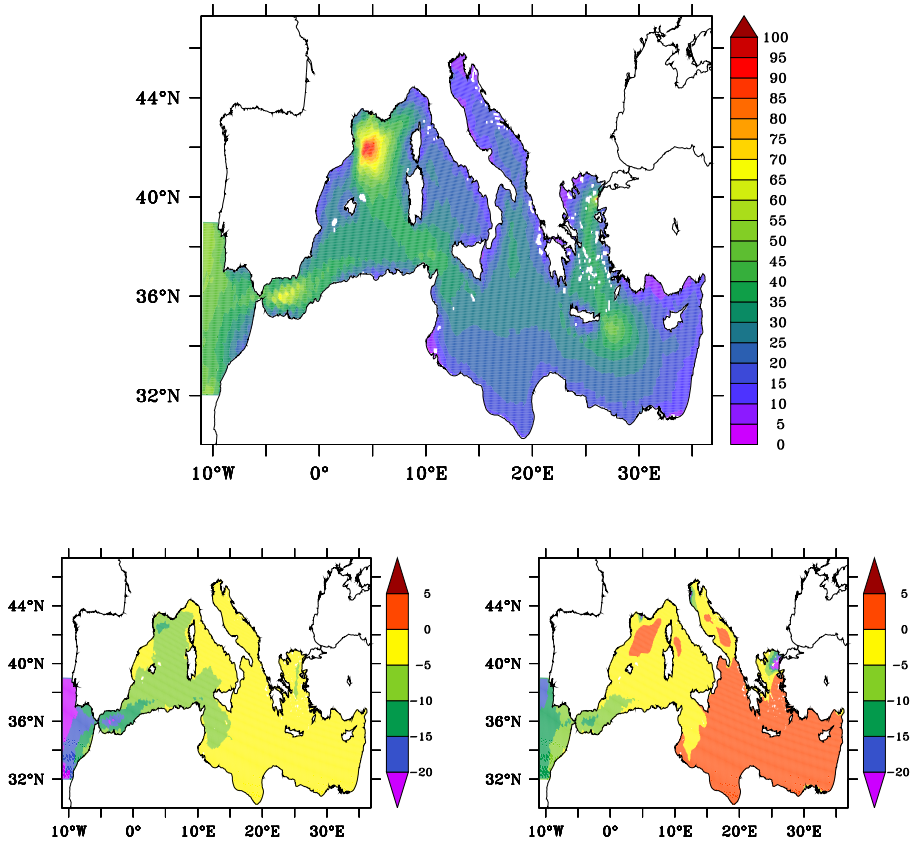

Fig. 7. Cumulative air-to-sea flux of anthropogenic carbon (mol m^{-2}) from 1800 to November 2001 shown as the total flux for the MED reference simulation (top) and for the other two simulations as differences: GLO – MED (bottom left) and VAR – MED (bottom right).

BGD
11, 6461–6517, 2014

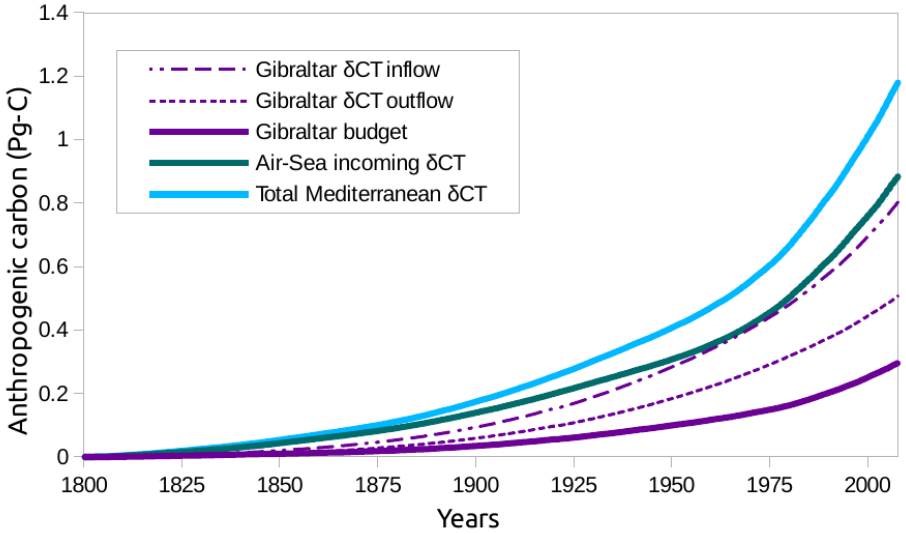

Fig. 8. Cumulative increase in anthropogenic carbon (Pg C) in the Mediterranean Sea from 1800 to 2008 due to the Gibraltar inflow (large dashed and dotted, purple) and outflow (dashed, purple), i.e., their difference (inflow – outflow, solid, purple), and the air–sea flux (solid, green). Also shown is the total buildup in inventory (solid, light blue).

BGD
11, 6461–6517, 2014

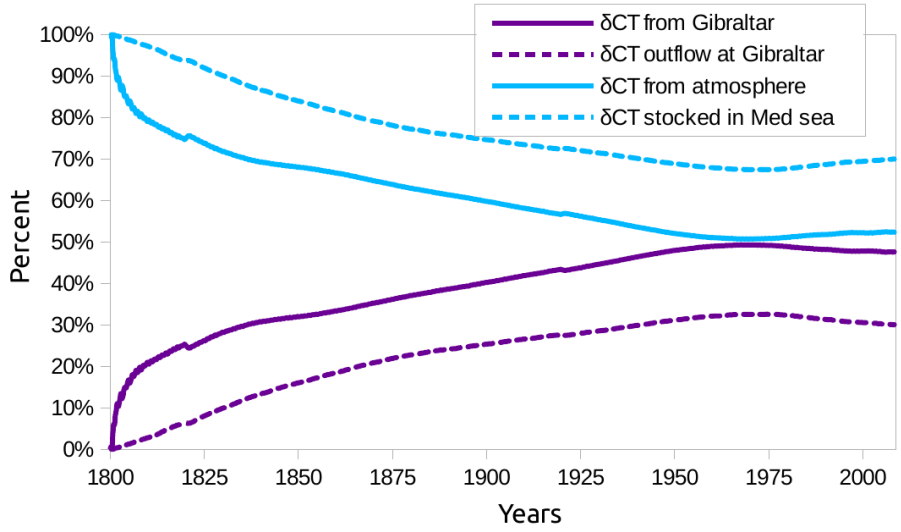

Fig. 9. Evolution of the percentage of the total δC_T that entered the Mediterranean Sea from the air–sea flux of anthropogenic carbon (solid, light blue) and from Strait of Gibraltar (solid, purple) minus that which leaves via the same strait but deeper down (dashed, purple). Also shown is the Mediterranean Sea's total storage (dashed, light blue).

BGD
11, 6461–6517, 2014

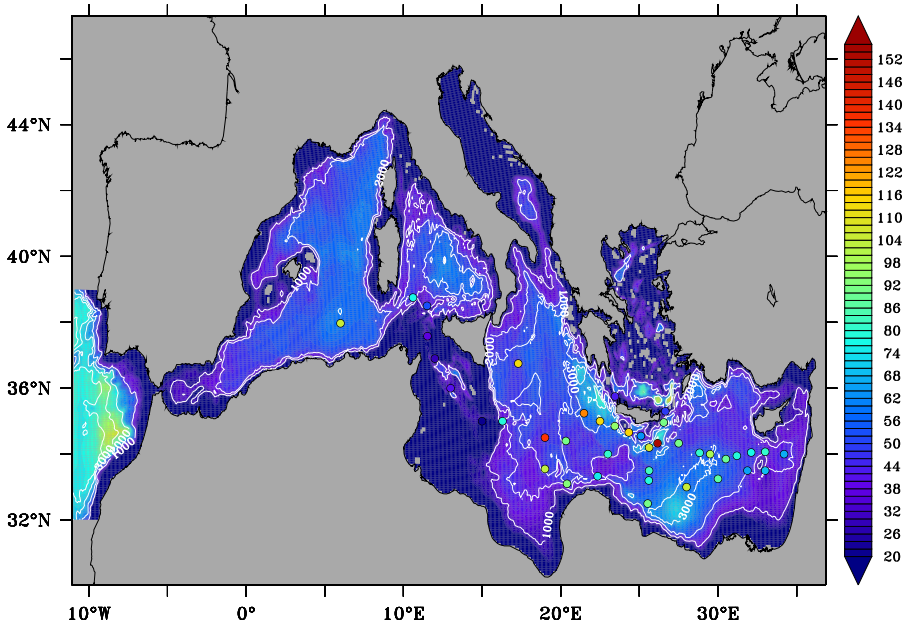

Fig. 10. Inventory of δC_T (mol m^{-2}) in November 2001 from the MED simulation (color-filled contours) and from Schneider et al. (2010) data-based estimates (color-filled dots). The Mediterranean bathymetry is represented with white isobaths every 1000 m.

BGD
11, 6461–6517, 2014

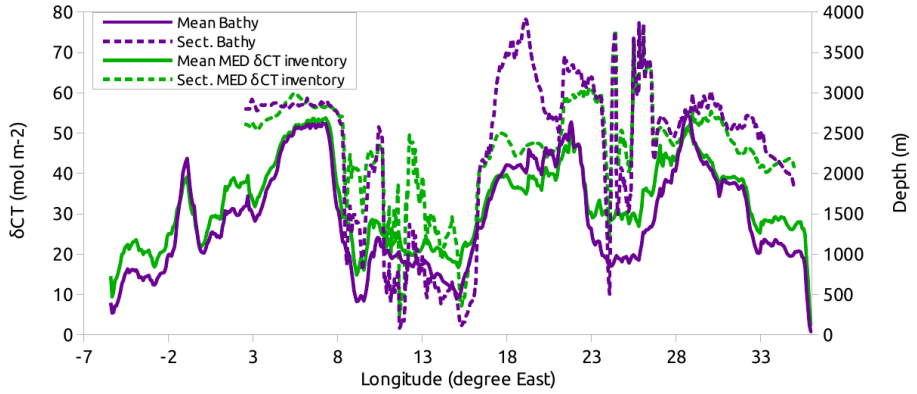

Fig. 11. δC_T inventory (mol C m^{-2}) along the METEOR M51/2 section (dashed lines) and given as the meridional mean (solid lines) for the MED simulation (green) along with corresponding model bathymetry (purple).

BGD
11, 6461–6517, 2014

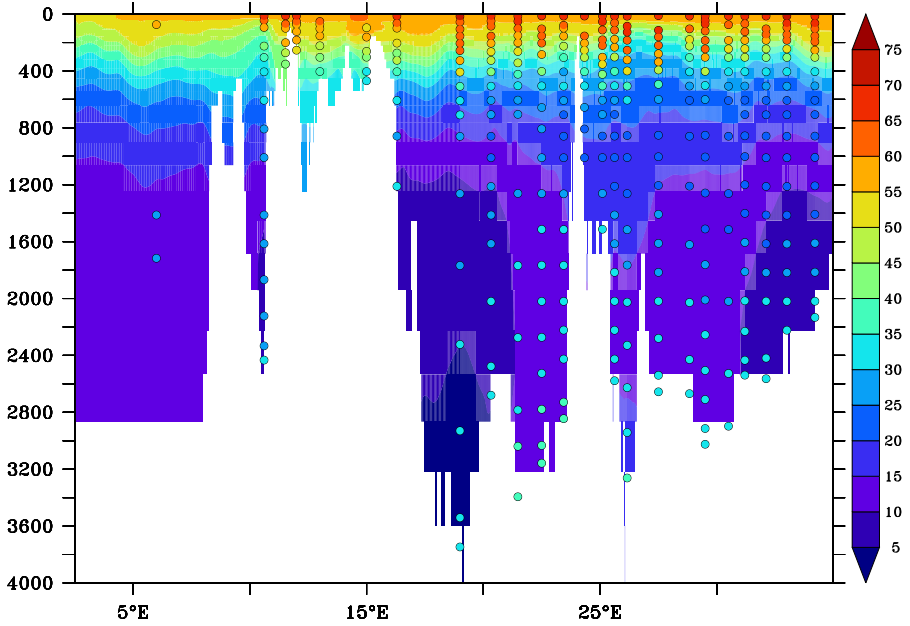

Fig. 12. Comparison of δC_T (µmol kg^{-1}) along the METEOR M51/2 section for the model (color-filled contours) and the TTD data-based estimates (color-filled dots) in November 2001.

BGD
11, 6461–6517, 2014

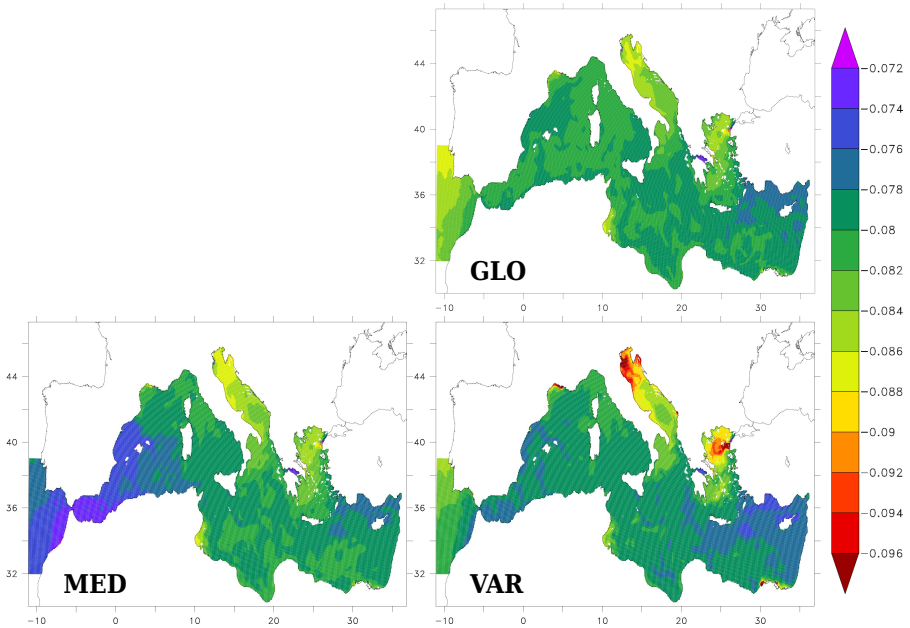

Fig. 13. Anthropogenic change in surface pH between 1800 and 2001 for the the GLO (top), MED (bottom left), and VAR (bottom right) simulations.

BGD
11, 6461–6517, 2014

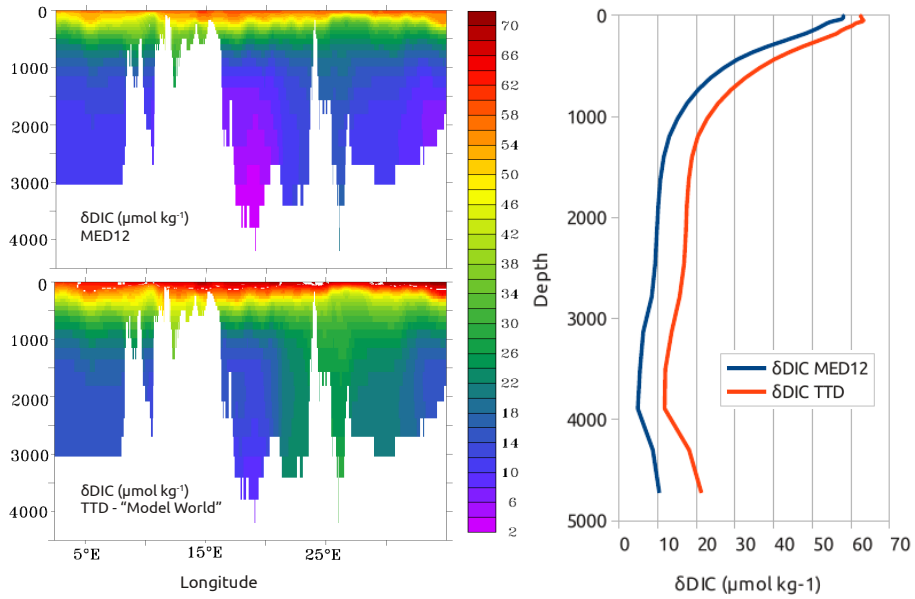

Fig. 14. δC_T (µmol kg^{-1}) along the METEOR M51/2 section, estimated with the MED reference simulation (top left) and the TTD method in the model world (bottom left). Also shown are the same results but as area-weighted vertical profiles for the whole Mediterranean Sea (right).

BGD
11, 6461–6517, 2014

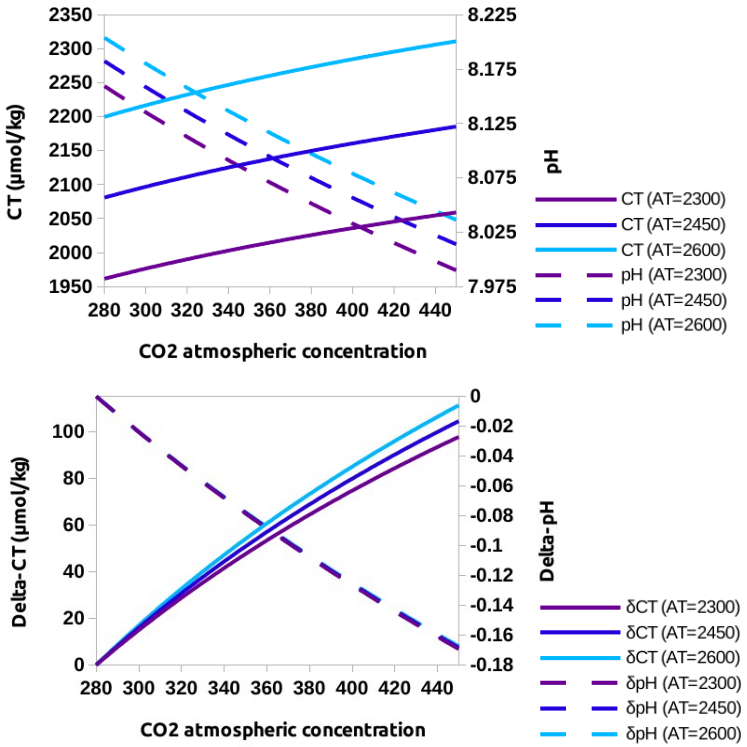

Fig. 15. Time evolution of C_T (solid) and pH (dashed) based on simple thermodynamic equilibrium calculations with seacarb (Lavigne and Gattuso, 2011) that vary atmospheric CO_2 (280 to 450 ppm) with 3 different fixed values of total alkalinity: 2300 (purple), 2450 (blue) and 2600 µmol kg^{-1} (light blue). The top panel shows the absolute values, whereas the bottom panel shows the change (anthropogenic perturbation relative to 280 ppm).

BGD
11, 6461–6517, 2014

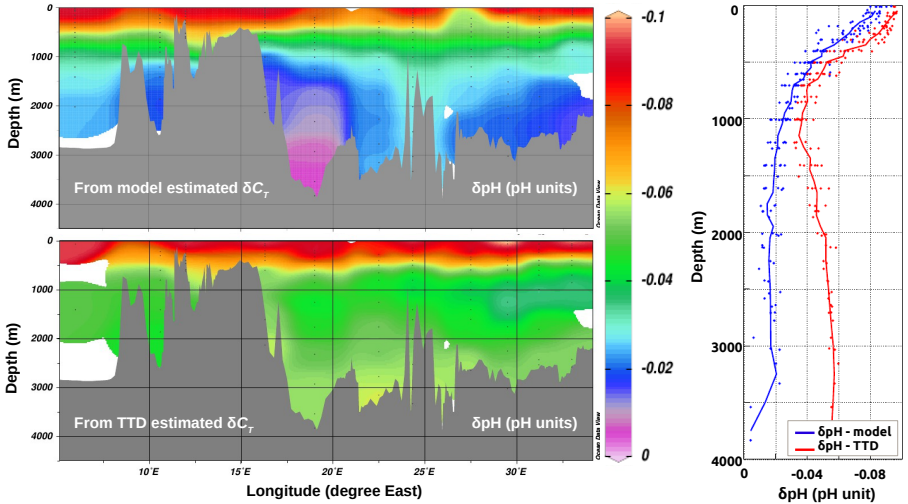

Fig. 16. Mediterranean δpH along the METEOR M51/2 section, calculated with δC_T from the MED simulation (top left) and from the TTD data-based estimates from Schneider et al. (2010) (bottom left). Also shown are the same results but as mean vertical profiles averaged along the section (right).

BGD
11, 6461–6517, 2014